ANISOTROPIC MAGNETIC SUSCEPTIBILITIES OF VANADIUM AND TITANIUM IONS IN CORUNDUM

by

ALFRED RICHARD SMITH, B.A., M.S.

A DISSERTATION

IN

PHYSICS

Submitted to the Graduate Faculty
of Texas Tech University in
Partial Fulfillment of
the Requirements for
the Degree of

DOCTOR OF PHILOSOPHY

May, 1970

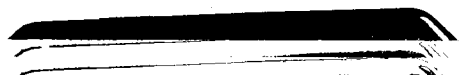

ACKNOWLEDGMENTS

I am deeply indebted to Dr. R. W. Mires who suggested and directed this work and was responsible for its financial support through a research grant from the Advanced Research Projects Agency. Dr. C. R. Quade and Dr. C. C. Lin furnished the crystals and Dr. Quade made many helpful suggestions. Appreciation is also extended to my co-workers. Don Arnold furnished the reference measurements and contributed to the work in many significant ways. Allan Wise, Ron Johnson, Morris Greenwood, and Bill Dean gave technical assistance in apparatus construction, data taking, and computer programming.

TABLE OF CONTENTS

LIST OF FIGURES

LIST OF TABLES

CHAPTER I

INTRODUCTION

The study of transition-metal ions in host crystals has made significant progress in recent years. The main impetus for this progress has been provided by new techniques for growing high quality single crystals with controlled amounts of impurities, and new experimental techniques such as high resolution spectrophotometry and electron paramagnetic resonance (EPR). Paramagnetic resonance[1] and optical[2] data have played a major role in the development of crystal field theory. However, in order to construct a complete description of the ions in their crystalline environment it has proven to be advantageous to employ the results of other experiments. Among the most important of these are magnetic susceptibility[3,4] measurements.

Paramagnetic resonance is most useful in the study of the lowest lying energy levels and in the determination of the g-factors and the energy level splittings of the ground state in a magnetic field.

Optical absorption spectra can be used to determine the higher lying crystal field levels between about 2000 cm^{-1} and 30,000 cm^{-1}. The crystal field parameters, the Slater-Condon parameters, and in some cases the spin-orbit coupling constants can be estimated from optical data. Estimates of the lower lying energy levels can also be obtained indirectly from this technique. Recently, far-infrared absorption spectra[5] in the 5-120 cm^{-1} range have been used to determine the low lying energy levels, g-factors, and Zeeman splittings of the ground state.

Magnetic susceptibility studies are useful in energy level determinations intermediate between those obtainable from paramagnetic resonance and optical data. In conjunction with other measurements it is possible to obtain such quantities as g-factors, trigonal field parameters, and spin-orbit coupling constants from susceptibility measurements.

Magnetic susceptibility data are especially interesting because a complete analysis depends in part upon parameters determined from other experiments. Therefore, the results of several areas of investigation can be combined in order to determine a complete and consistent set of parameters which provide a solution to the crystal-ion problem. In Chapter II the general theory of the transition-metal ion in the environment of host crystals is presented. The Hamiltonian is given along with a discussion of the effects of its perturbation terms on the energy levels of the free ion. The general expression for the calculation of magnetic susceptibilities is also derived.

If a magnetically anisotropic sample is placed in an inhomogeneous magnetic field, the direction of the field being along one of the crystal axes, a force is exerted on the sample which is proportional to the magnetic susceptibility along that axis. If the sample is placed in a homogeneous field, a torque is exerted on it which is proportional to the difference between the susceptibilities perpendicular and parallel to the axis along which the field is applied. Therefore, magnetic susceptibility measurements fall into two general classes: Force measurements, which determine the absolute suscep-

tibilities, and torque measurements, which determine the anisotropic susceptibility. This study is concerned with the measurement of the anisotropic susceptibility of ions in host crystals. Chapter III is devoted to a description of the torsion balance used for these measurements along with a discussion of the experimental techniques involved.

Chapters IV and V contain the results of magnetic susceptibility measurements on samples of $Al_2O_3:V^{3+}$, and $Al_2O_3:Ti^{3+}$, and an analysis of the data. The analysis consists primarily of fitting the data and theory by least squares methods in order to determine various parameters which arise in the development of the theoretical expressions for the energy levels of the systems. The last chapter contains a summary of the results of this study and the conclusions based on these results.

CHAPTER II

GENERAL THEORY

Crystal field theory has been successful in explaining many of the experimental results of studies on inorganic complexes. A complex molecule will be considered here as being any compound containing a central metal ion surrounded by a cluster of ions or molecules. It is customary to call the central ions "cations" and the ions or molecules surrounding the central ion "ligands."

This work is concerned with complexes obtained by substituting dilute quantities of vanadium or titanium into an Al_2O_3 host. These metals enter the corundum lattice substitutionally for the Al^{3+} ions. In the corundum structure the V^{3+} and Ti^{3+} cations are coordinated by trigonally distorted octahedra of diamagnetic O^{2-} ligands.[6] For dilute doping the nearest cation neighbors to the impurity ions should be Al^{3+} ions which are also known to be diamagnetic.[7]

A short history of the crystal field theory is given in a text by Ballhausen[8] which discusses the important contributions to the development of the theory. Of particular interest is the work of Schlapp and Penney[9] and of Jordahl[10] who showed that both the anisotropy and the variation of the magnetic susceptibility with temperature could be exactly predicted and calculated from the crystalline field model.

The basic idea of the crystal field theory is that the metal ion in the complex is subjected to an electric field originating from the

surrounding ligands. The electrons on the ligands are assumed not to overlap and mix with the electrons of the metal ion. The ligands can be polarized by the metal ion of the complex, but the motions of their electrons are assumed to remain unaffected by such factors as whether or not the electrons of the metal ion are in an excited state. Thus the ligands are assumed to provide only an electrostatic potential possessing the symmetry of the arrangement of the ligand nuclei.[11]

The crystalline field reduces the symmetry of the free ion environment, and thereby reduces the degeneracy of the electronic levels. Van Vleck[12-14] demonstrated the superiority of the crystal field approach over the old valance-bond theory of Pauling[15] in explaining the magnetic properties of inorganic complexes. Van Vleck was the first to realize that the effect of the crystal field would lead to a quenching of the orbital angular momentum, and thus explain why the paramagnetism of the complexes of the first transition series corresponds to a "spin-only" value.[3]

The Hamiltonian for the free metal ion is

$$H_F = \frac{-\hbar^2}{2m} \sum_i \nabla_i^2 - \sum_i \frac{Ze^2}{r_i} + \frac{1}{2} \sum_{i \neq j} \frac{e^2}{r_{ij}} + \sum_i \xi_i(r) \vec{l}_i \cdot \vec{s}_i, \qquad (1)$$

where the sums are over the individual electrons of the impurity ion. Only relative energies are significant for the magnetic properties and since the sums over closed-shell electrons contribute a constant term which shifts all configurations by a constant amount these terms are neglected. The sum is then taken over (3d) electrons outside the closed argon shell. It is assumed that the eigenvalues and eigen-

functions of this Hamiltonian are known.[16]

The one-electron terms comprising the unperturbed Hamiltonian,

$$H_F^o = \frac{-\hbar^2}{2m} \sum_i \nabla_i^2 - \sum_i \frac{Ze^2}{r_i}, \tag{2}$$

are the kinetic and potential energy operators, respectively, while the two electron operators,

$$e^2/r_{ij}, \tag{3}$$

arise from the electrostatic repulsion forces between the electrons. The terms,

$$\xi_i(r)\vec{l}_i \cdot \vec{s}_i, \tag{4}$$

are the spin-orbit operators arising from the interaction of the magnetic moment associated with the intrinsic spin of the electron and the magnetic moment produced by the electronic orbital motion.[4] The interaction of a spin with orbits other than its own is neglected. $\xi_i(r)$ is the one-electron spin-orbit parameter and $\vec{l}_i$ and $\vec{s}_i$ are the orbital angular momentum and spin angular momentum, respectively, of the individual electrons.

In complexes of the first transition series the effect of the crystal field is small with respect to the separation of the atomic multiplets of the free metal ion but is large with respect to spin-orbit interactions. Therefore,

$$\xi(r)\vec{l} \cdot \vec{s} < V < e^2/r_{ij}, \tag{5}$$

where V is the effect of the crystalline field. This is called the "weak-field case," and in formulating the problem the weak-field approximation is used in which the electrostatic energies between the electrons, Eq. (3), are included in the unperturbed Hamiltonian of the free ion, Eq. (2), and configuration interaction with higher terms is neglected.[8] The Hamiltonian can therefore be written,

$$H = H_o + V + \sum_i \xi_i(r)\vec{l}_i \cdot \vec{s}_i, \tag{6}$$

where,

$$H_o = \frac{-\hbar^2}{2m} \sum_i \nabla_i^2 - \sum_i \frac{e^2}{r_i} + \frac{1}{2} \sum_{i \neq j} \frac{e^2}{r_{ij}}. \tag{7}$$

The eigenfunctions of H_o associated with the various multiplet components are taken as the usual Clebsch-Gordan combinations of the one-electron orbitals.[16]

For a given L-S state (assuming Russell-Saunders coupling) where L is the total orbital angular momentum and S is the total spin, the matrix elements of the spin-orbit operator,

$$H_{s-o} = \sum_i \xi(r_i)\vec{l}_i \cdot \vec{s}_i, \tag{8}$$

are proportional to the matrix elements of $\vec{L} \cdot \vec{S}$.[8] Therefore the operator can be written,

$$H_{s-o} = \lambda \vec{L} \cdot \vec{S}, \tag{9}$$

where the radial integrations have now been included in λ, the spin-orbit coupling constant.

If the effect of an applied magnetic field is included, the final Hamiltonian becomes

$$H = H_o + V + \lambda \vec{L} \cdot \vec{S} + \mu_o (\vec{L} + 2\vec{S}) \cdot \vec{H}. \tag{10}$$

The last term is the operator associated with the Zeeman energy, where μ_o is the Bohr magneton and $\vec{H}$ is the applied magnetic field. This is the paramagnetic part of the Zeeman energy. The diamagnetic contribution is small and for atoms not in ^1S states it is negligible compared to the paramagnetic part.[4]

The Hamiltonian given by Eq. (10) has been successful in explaining the optical and magnetic properties of some transition-metal complexes, while in others, some modification is required. It has been customary to rationalize the discrepancies between experiment and thoery by introducing covalent bonding[17] or Jahn-Teller effects[18] or both. In $Al_2O_3:V^{3+}$, it is possible to fit the magnetic properties with the crystal field parameters alone, while in $Al_2O_3:Ti^{3+}$ it is necessary to include the dynamic Jahn-Teller effect to adequately explain the experimental results. Only the theory relevant to both systems will be discussed here; individual considerations will be taken up in the appropriate sections of Chapters IV and V.

The crystal field potential of Eq. (10) is

$$V = \sum_i V(r_i, \theta_i, \phi_i), \tag{11}$$

where the sum is over all the electrons of the central metal ion. Since the symmetry at the site of the metal cations is primarily cubic with a small trigonal distortion[2,4,8] it is assumed that the potential can be decomposed into two terms corresponding to the cubic potential and trigonal potential, i.e.,

$$V(r_i,\theta_i,\phi_i) = (V_i)_c + (V_i)_t, \tag{12}$$

where V_t is much smaller than V_c. The field of the six point charges surrounding the central metal ion may be represented by an expansion in spherical harmonics about the central ion as origin. It must be assumed in making this expansion that the potential obeys Laplace's equation, and therefore that the d-orbitals of the metal ions do not overlap the charges. The Hamiltonian corresponding to this potential is

$$V(\vec{r}) = \sum_n \sum_{m=n}^{-n} \sum_j A_n^m \, r_j^n \, Y_n^m(\theta_j,\phi_j), \tag{13}$$

where j runs over all the electrons of the central ion. The largest term of the potential is the n = 0 term to which the core electrons contribute. This term is a constant and will shift all levels in all configurations by the same amount. Since only relative energies are significant for the magnetic properties the constant term is neglected. The ground state configurations for V^{3+} and Ti^{3+} are $[A](3d)^2$ and $[A](3d)^1$, respectively, where [A] is the closed argon shell. For d electrons the triangle rule of spherical harmonics rules out n > 4

and inversion symmetry rules out odd n when matrix elements of the crystal field operators are calculated. Therefore for the first-transition series only n = 2 and n = 4 need be considered. This gives

$$V_c = \sum_{i=1} A_4^o \, r_i^4 \, \{Y_4^o(\theta_i,\phi_i) + (10/7)^{1/2}[Y_4^3(\theta_i,\phi_i) - Y_4^{-3}(\theta_i,\phi_i)]\}, \quad (14)$$

and

$$V_t = \sum_{i=1} B_2^o \, r_i^2 \, Y_2^o(\theta_i,\phi_i) + B_4^o \, r_i^4 \, Y_4^o(\theta_i,\phi_i), \quad (15)$$

with the z axis along the crystal c-axis. The A_n^m and B_n^m along with the radial integrals over the r_i^n are treated as parameters to be determined from the optical data.

The usual method of finding solutions to Eq. (10) is to diagonalize the Hamiltonian through V_c, then obtain the matrix elements of the remaining terms in the cubic-field representation. A Van Vleck transformation[19] is usually used to facilitate the solution of the resulting secular equation.

Group theory[4,8] is useful in determining how the various levels will split and what the resulting degeneracies are. The general effect of all the perturbation terms is a splitting and/or shifting of the energy levels with a subsequent partial or total removal of the degeneracy of the level.

Suppose the energy levels for an ion are known, or that the theoretical expressions have been developed by crystal field theory. The energy, W_n, of an ion can be expanded in a series in the applied

field H,

$$W_n = W_n^o + HW_n^{(1)} + H^2W_n^{(2)} + \ldots, \tag{16}$$

where n specifies the quantum numbers characterizing a stationary state and W_n^o is the energy in zero magnetic field. The magnetic moment μ_n of the ion in the direction of the applied field is

$$\mu_n = -\partial W_n/\partial H. \tag{17}$$

In the presence of the magnetic field there is a thermal distribution of aligned dipoles in the various energy levels. The total magnetic moment, M, per gram ion is then found as the statistical average over all the stationary states, using a Boltzmann distribution,

$$M = N \frac{\Sigma_n \mu_n \exp(-W_n/kT)}{\Sigma_n \exp(-W_n/kT)}, \tag{18}$$

where N is the number of ions. There is often confusion as to why Boltzmann statistics are used here. Electrons obey Fermi-Dirac statistics, and it is supposed that the electrons in the metal ion definitely obey the Pauli exclusion principle in so far as they compete with each other for quantum states within the ion. Once the paramagnetic properties of the ion are so determined, however, the assumption of independent noninteracting ions implies a spatial separation and, in effect, a spatial distinguishability of particles. This spatial distinguishability means that Boltzmann statistics are appropriate.[20]

Substitution of Eqs. (16) and (17) into Eq. (18), expansion of the exponentials assuming kT >> W(H), and the further assumption that the ion has no permanent magnetic moment, lead to the quantum mechanical expression,[3]

$$\chi = \frac{N\Sigma_n g_n [(W_n^{(1)})^2/kT) - 2W_n^{(2)}]\exp(-W_n^o/kT)}{\Sigma_n g_n \exp(-W_n^o/kT)}, \qquad (19)$$

where the component of the susceptibility, χ_i, in a given direction (i = x,y,z) is given by $\chi_i = M_i/H_i$. g_n is the multiplicity of the state n.

If sufficient optical data are available to determine the parameters imposed by the crystal field model, it is possible to predict the magnetic behavior of the lower levels without introducing further parameters. Alternatively, the magnetic properties may be used to determine crystal field parameters, in cases where the optical transitions are either forbidden or are not clearly assigned.

CHAPTER III

GENERAL DISCUSSION OF THE EXPERIMENT

The Torsion Balance

A magnetically anisotropic sample in a homogeneous magnetic field experiences a torque which is proportional to $\Delta\chi \equiv \chi_{\perp} - \chi_{//}$, where $\chi_{\perp}$ and $\chi_{//}$ are the magnetic susceptibilities perpendicular and parallel to the c-axis of the crystal, respectively. To measure $\Delta\chi$ a torsion balance (shown in Figure 1) has been constructed. The homogeneous magnetic field is produced by a rotating Varian 4 inch electromagnet (M) with its regulated power supply and heat exchanger.

The principal part of the torsion balance consists of a converted Dolezalek quadrant electrometer (E). It is supported by a copper pump plate (G) and enclosed by a bell jar (F). A rubber gasket provides a vacuum seal between the pump plate and the bell jar.

Vacuum connections are made to the pump plate to accommodate a 160 ℓ/m mechanical vacuum pump, an inlet for helium exchange gas, an outlet for attaching a thermocouple vacuum gauge, and an outlet to a mercury manometer. The vacuum gauge is used to measure pressures in the 0-1000 micron range and the mercury manometer is used to measure pressures from 1000 microns to atmospheric. Electrical feedthroughs soldered into the pump plate provide a means to pass voltages from the outside to the electrometer. A vacuum connection (H) of the type normally used to connect ion gauges to vacuum systems is soldered to the under side of the pump plate. This connection provides support

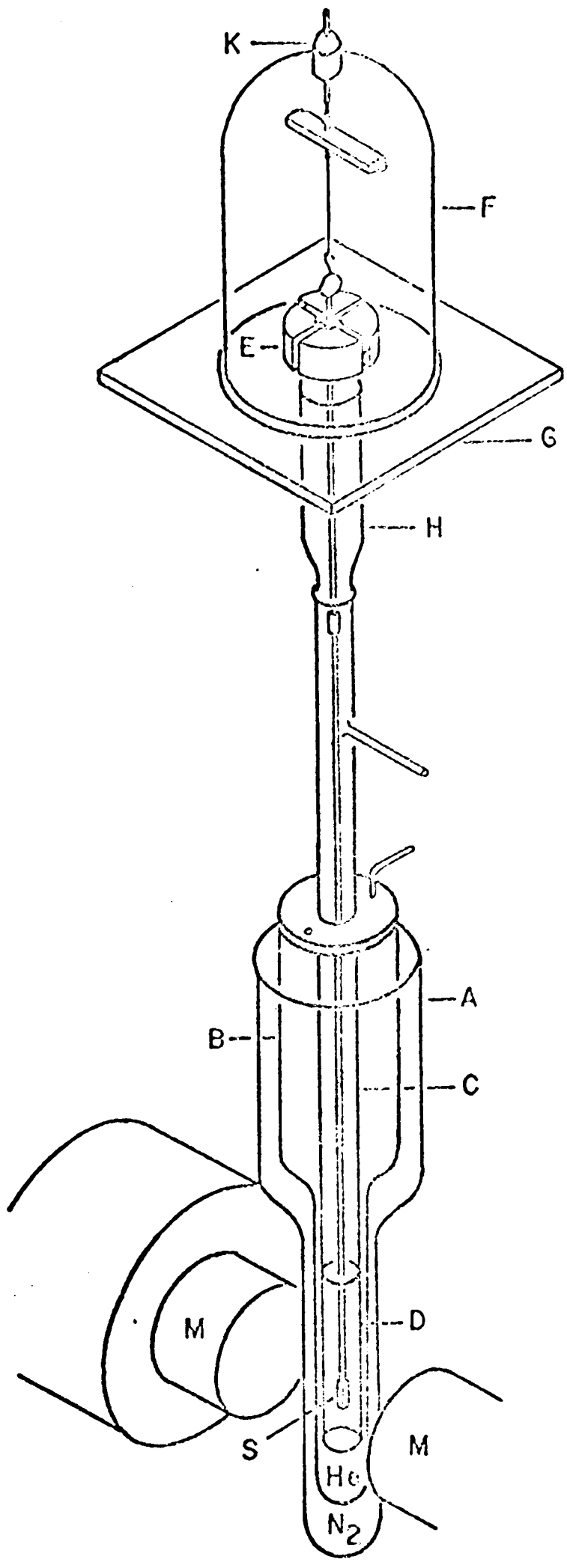

Figure 1: Diagram of the Anisotropy Torsion Balance.

and vacuum seal for a 16.5-mm diameter hang-down tube (C) hanging vertically between the pole pieces of the magnet. An opening in the top of the bell jar is fitted with a screw-type adjustment (K) linked mechanically to an adapter fastened to the manual adjustment knob of the electrometer. This device is vacuum sealed and it provides a means of zeroing the electrometer from the outside.

A 1-mm diameter quartz rod, 22-cm long is glued to the under side of the electrometer vane. The lower end of this rod, which hangs just below the vacuum connection for the hang-down tube, is connected to a second quartz rod, 72-cm long, by means of a non-rotating hook assembly. The lower end of the longer rod is fused to a 4-mm square quartz plate to which the sample (S) is attached.

The suspended sample hangs inside an oven (D) at the lower end of the hang-down tube. The oven consists of No. 36 nichrome wire, with 26.20 ohms per ft., wound non-inductively on a thin-walled, cylindrical teflon form about 10-cm long. The sample hangs in the center of the oven a few millimeters above a copper-constantan thermocouple junction and a germanium resistance thermometer. The thermocouple junction and resistance thermometer are in thermal contact with each other but are insulated from the oven by a rubber holder which fits into the bottom of the oven. The germanium resistance thermometer is used for temperature measurements in the 0-30 K range and the thermocouple is used in the 30-400 K range.

The thermocouple, resistance thermometer, and oven electrical leads pass up the hang-down tube inside two 1.7-mm diameter Pyrex tubes held to the side of the hang-down tube by copper spacers. The

electrical leads pass to the outside through outlets near the top of the hang-down tube. The outlet tubes are filled with Cenco Softseal vacuum wax after the leads are in place, then the ends of the tubes are sealed with Gevac vacuum leak sealer.

The hang-down tube is suspended inside a liquid helium Dewar (B) and a liquid nitrogen Dewar (A). The top of the liquid helium Dewar is fitted with a copper vacuum jacket. An O-ring provides a vacuum seal between the jacket and hang-down tube, and a larger O-ring provides a vacuum seal between the helium Dewar and the jacket. The copper jacket has connections for attaching a 500 ℓ/m mechanical vacuum pump, a thermocouple vacuum gauge, and a manometer to the liquid helium system, and has an O-ring sealed opening in the top to accommodate a liquid helium transfer tube.

The Dewar system is supported by a platform built over the magnet (not shown in Figure 1). The Dewar support is attached to a rail assembly so that the Dewar can be slid in and out under the balance, and it has slot adjustments for leveling and alignment purposes. The balance itself is supported by an aluminum plate attached to two lab jacks, one on each side of the rail assembly. Thus, the balance can be raised away from the Dewar system, the quartz rods unhooked, and the Dewar system slid forward on the rails to change samples or to remove the hang-down tube. Three adjustment screws on the legs of the balance permit leveling and alignment so that the two parts of the system can be matched.

An aluminum wire about 6-cm long soldered to the top of the electrometer vane is connected to the lower end of the torsion fiber,

which is suspended from the upper swivel assembly of the electrometer. The torsion fiber is a flat, gold strip of the type used in galvanometers. Another length of aluminum wire is soldered horizontally to the vertical aluminum wire about 3-cm above the quadrants. This wire is bent 90° downward about 1-cm from the junction on each side, and the ends of the wire are fashioned into small loops. These loops hang mid-way into a hollow, doughnut shaped, teflon damping cup which is cemented to the top of the quadrants. The damping cup is filled with Silicone D.C. 703 oil. In order to prevent frothing of the oil when the chamber is evacuated, it is necessary to de-gas the damping fluid by heating under vacuum. This damping cup serves a two-fold purpose. First, the system is slightly underdamped so that equilibrium is essentially reached after one cycle of oscillation, thus sequential measurements can be taken quite rapidly. Second, the damper helps to smooth out fluctuations in the balance displacements caused by convection currents in the hang-down tube.

A small, plane, circular mirror is attached vertically with wax to the vertical aluminum wire about 5-mm above the damper wire so that the mirror rotates about the axis of the balance when a torque is applied. The optical system of the balance is shown in Figure 2.

The light from a concentrated argon filled, zirconium-arc, lamp (E) is focused onto the eyepiece of a telescope (C) by means of a convex lens (D). The telescope superimposes a hair-line onto the beam, the image of which is reflected by the balance mirror (A) onto the curved scale (B). The distance between the mirror and the scale is approximately 2-m which allows very small deflections of the mirror

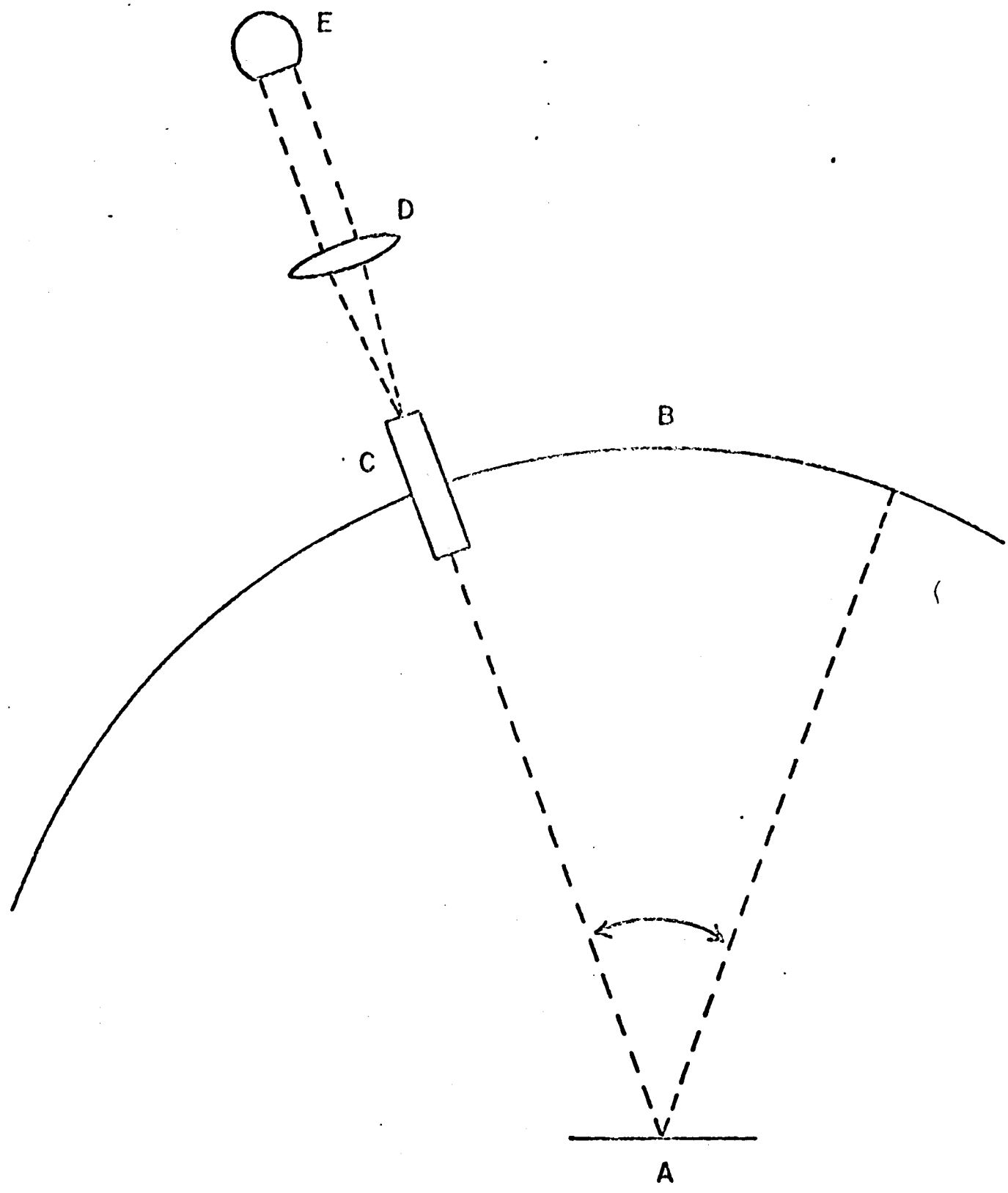

Figure 2: Optical System of the Balance.

to be observed. The optical equipment is attached to an optical bench to permit the sensitive alignment and stability required for the experiment.

A block diagram of the electrical circuitry for the torsion balance is shown in Figure 3. Two of the opposing quadrants of the electrometer are grounded, while voltages are applied to the other two quadrants and the vane. The 10 megohm resistor is used to prevent arcing in case the vane should touch one of the quadrants. A Dolezalek electrometer wired in this manner is said to be wired heterostatically and the equation for the torque is[21]

$$L_E = -cV_q(V_v - V_q/2), \tag{20}$$

where c is a constant depending upon the geometry. V_q and V_v are the potentials of the quadrants and vane, respectively, with respect to ground.

Figure 4 shows a detailed schematic of the power supply built for the electrometer. It consists of eight 45 volt dry cells and one 1.5 volt cell in series, wired to the ganged switch SW-1. The ganged switch permits selection of voltages in steps of 45 volts to be applied to the quadrants. The 100 K, 10-turn Helipot permits a 0-45 volt adjustment of each successive 45 volts applied to the quadrants. In this manner the voltage has continuous adjustment from 0-360 volts (not including the 1.5 volt cell), while only 45 volts are applied to the Helipot at any time. This greatly reduces the current drain on the batteries, and permits good stability of the batteries which

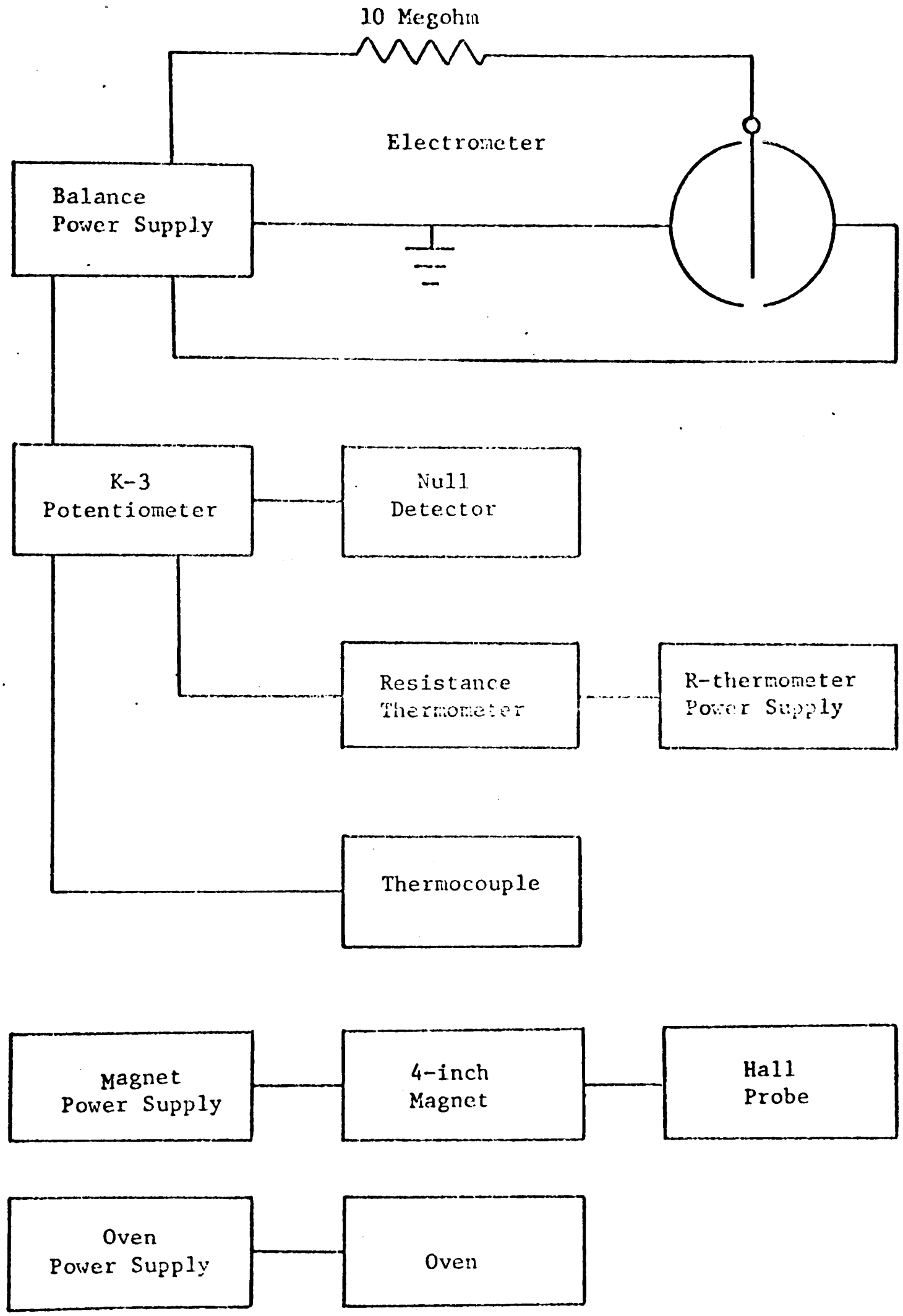

Figure 3. Block Diagram of the Electrical Circuitry of the Balance.

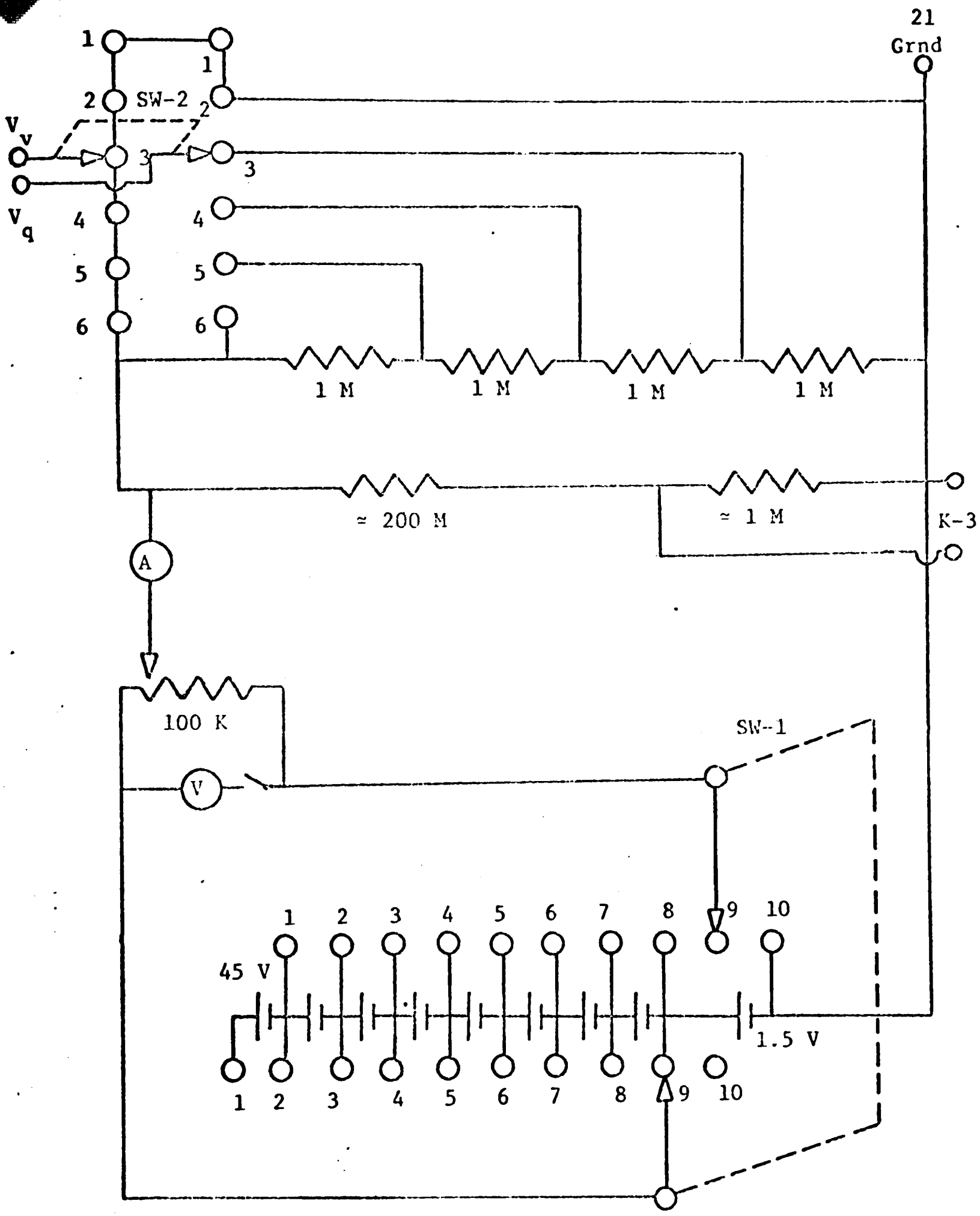

Figure 4. Schematic of Balance Power Supply.

is essential because of the time required to make a measurement. A voltmeter and switch across the Helipot permits a check of the voltage and stability of each individual battery. A portion of the voltage applied to the quadrants is picked off by a voltage divider for measurement by the K-3 potentiometer. Calibration of the voltage divider shows that this voltage is $V_q/213.508$. The quadrant voltage is reduced in this manner so that the voltage can be applied directly to the K-3, bypassing a volt-box which is required for the measurement of voltages above 1.6 volts. The volt-box causes excessive current drain on the batteries and makes the voltage unstable. The voltage divider permits a potentiometric voltage measurement.

The voltage dividing network consisting of four calibrated 1 megohm resistors, and the ganged switch SW-2, supplies voltages of 0, 0.25, 0.50, 0.75, and 1.00 times V_q to the vane of the electrometer. From Eq. (20) we see that this will produce a change in torque from $L_E = cV_q^2$ to $L_E = -cV_q^2$. Therefore, this switching arrangement, coupled with SW-1 and the Helipot, permits the torque to be adjusted continuously between $\pm cV_q^2$. These limits, for the available V_q, are adequate for the samples and field values used in this study. The 1.5 volt battery is used to check the calibration of the voltage dividing networks. All of the dry cells are kept in a thermally insulated box to prevent voltage fluxuations due to changes in ambient temperature.

Temperature Measurement and Control

For measuring temperatures in the 0-30 K range a Cryocal germanium resistance thermometer was used. The physical location of the

thermometer was described in the last section. The thermometer was supplied by Cryocal with room temperature, liquid nitrogen dip, and liquid helium dip calibration points. The thermometer was further calibrated against a calibrated resistance thermometer manufactured by Cryocal, Inc. over the temperature range 1.72 - 24.6 K. For temperature measurements below 1.72 K and a few degrees above 24.6 K an extrapolation of this calibration was used.

The calibration method was as follows. The thermometer being calibrated was thermally coupled to the Cryocal standard in a copper block mounted within a controlled vacuum which was immersed in a liquid helium bath. Constant temperature conditions were reached and maintained for any desired temperature through a balance of low power electrical heating and the cooling provided by the controlled pressure of helium exchange gas. The electrical and thermal design of the cyrostat provided a minimum temperature difference within the calibration block.

Figure 5 shows a simplified schematic diagram of the power supply and control circuit for the germanium resistance thermometer and values of the resistances and currents for each temperature range. These values are chosen such that joule heating effects in the thermometer are minimized. All voltage measurements were made with a Leeds and Northrup K-3 potentiometer in conjunction with a L & N null detector.

In the calibration procedure the thermometers were wired in series and their separate emf's fed to the K-3 potentiometer through a L & N double-pole, double-throw, thermal switch. One side of the switch was used to monitor the current through the thermometers. The equa-

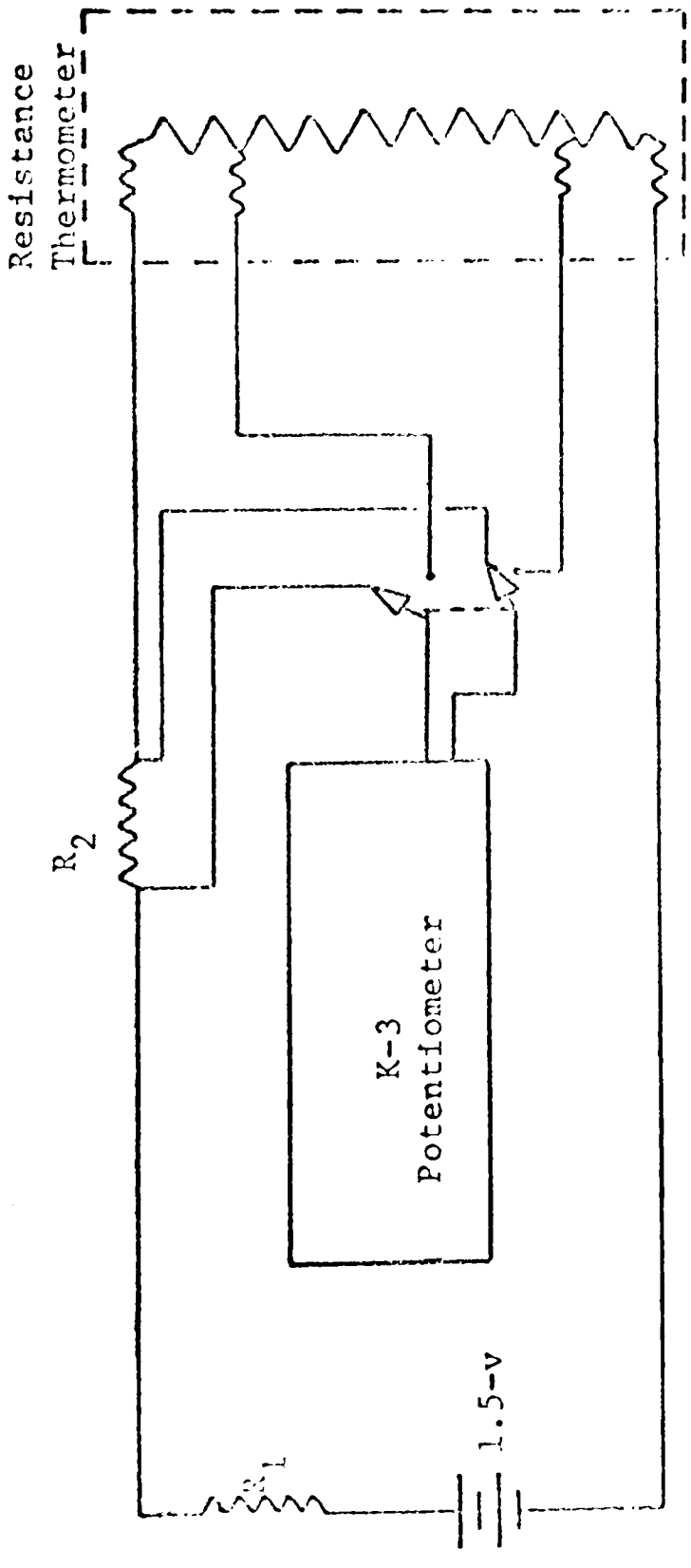

Temp °K	R_1	R_2	I
1-2	1.5M	10K 0.1%	1.0 a
2-15	150K	1000Ω 0.1%	0.01ma
15-40	15K	100Ω 0.1%	0.1ma
40-100	1.5K	10Ω 0.1%	1.0ma

Figure 5. Simplified Schematic of Germanium Probe Circuit.

tion for the thermometer resistance is

$$R_T = \frac{emf_T \times R_2}{emf_{R_2}} . \tag{21}$$

The accuracy of the K-3 potentiometer for the 0.016-mv or low range is ±(0.015% of reading +0.5μv), and the resistances R_2 were calibrated to ±0.1%. Hence, the thermometer resistance is

$$R_T = \frac{emf_T \pm (0.015\% + 0.5\mu v) \times (R_2 \pm 0.1\%)}{emf_{R_2} \pm (0.015\% + 0.5\mu v)} . \tag{22}$$

During calibration, the resistance of both thermometers was found at each temperature point. The standard data were taken before and after the data were taken for the thermometer being calibrated. The data for the standard were then averaged, and this average resistance matched with the resistance of the uncalibrated thermometer. The temperature was then found from a graph plotted from the resistance and temperature calibration points furnished for the standard by Cryocal. This temperature was then matched to the corresponding measured resistance of the thermometer being calibrated.

An error analysis based on Eq. (22) above, as well as the error in the calibration of the Cryocal standard, and plotting errors, resulted in errors of ±1.06% in the 1.5 to 2.0 K range, ±0.8% in the 2 to 5 K range, and ±1.0% in the 5 to 10 K range. Therefore, an error of ±1.0% in the temperatures obtained from measurements by the resistance thermometer is used in the analysis of the data. A further check

on the accuracy of the temperatures obtained from the resistance thermometer was made by comparing the temperatures obtained from the resistance thermometer against those obtained from measuring the vapor pressure of liquid helium at various points below 4.2 K and determining the temperature from He^4 vapor pressure tables obtained from the National Bureau of Standards. The agreement was always well within the ±1% error.

The copper-constantan thermocouple was used for temperature measurements above 30 K. The wires used were Leeds and Northrup size No. 30, standardized, with limits of error not exceeding 1%. The thermocouple emf's were measured by the K-3 potentiometer and the temperatures found from calibration tables furnished by L & N. The reference temperature was an ice bath maintained at 0.0 C. The thermocouple junction and the resistance thermometer were in thermal contact as described in the last section and the accuracy of the thermocouple was verified by comparing the measurements of the two sensors at low temperatures.

To make sure that the temperature sensors measured the temperature of the sample, helium exchange gas was used in the sample chamber. To find out what pressure of exchange gas was necessary to insure thermal equilibrium between the sample and the temperature sensors, the sample was replaced by a germanium resistance thermometer and the helium exchange gas pressure was varied while the two resistance thermometers were simultaneously monitored. Figure 6 shows the results of that experiment. The difference in the temperature readings of the two thermometers is plotted against the helium exchange gas pres-

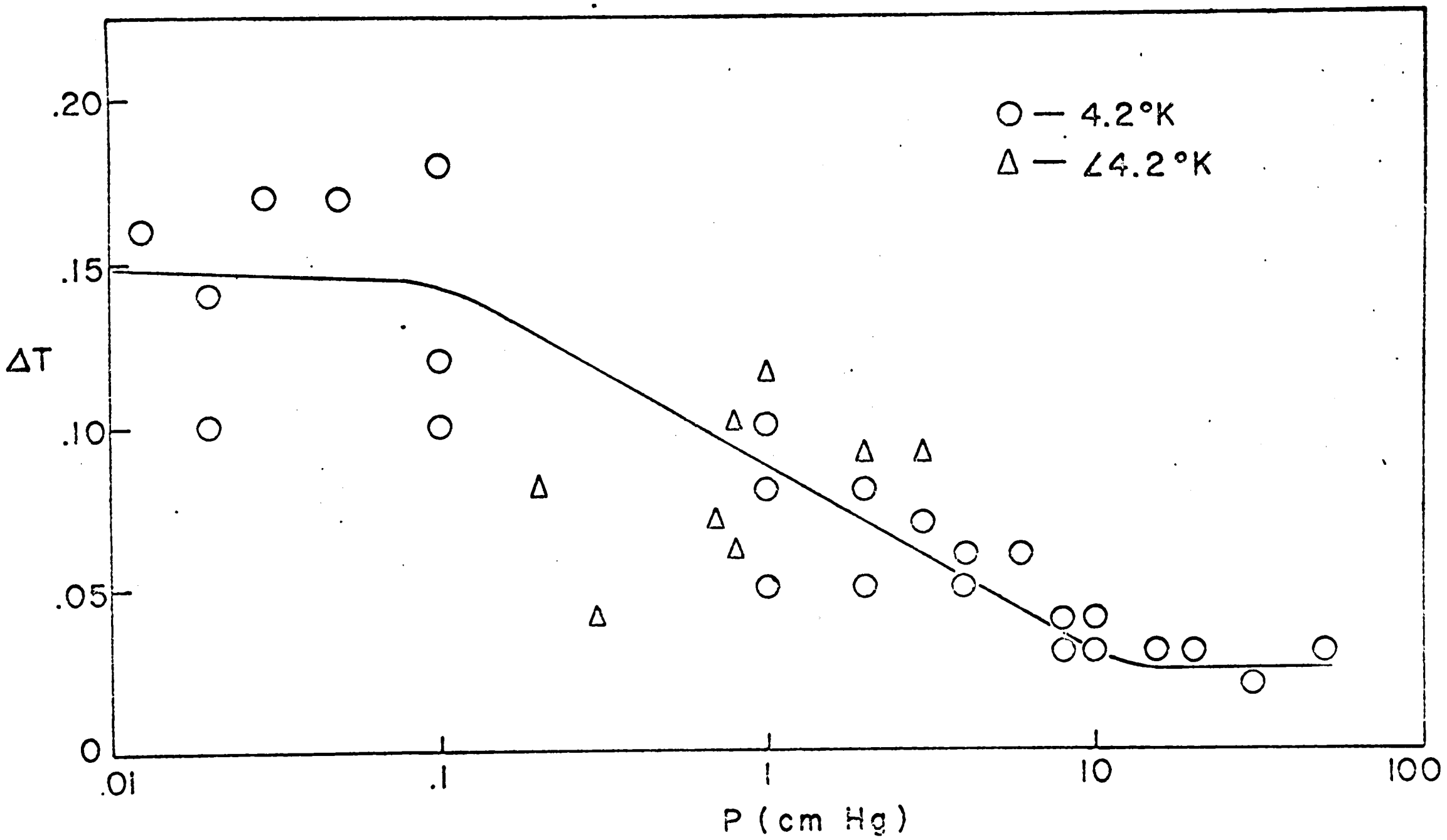

Figure 6. Temperature Difference Between Two Thermometers Versus Exchange Gas Pressure.

sure. The circles are data taken at the helium boiling point and the triangles are data taken at various lower temperatures obtained by pumping on the liquid helium with 10-cm Hg of exchange gas at 4.2 K. The data represent the results of several runs and the scatter of the points is attributed mainly to different time intervals between successive datum for each run. The solid line represents an approximate average of the 4.2 K runs. The results indicate that the two thermometers agree within their error limits (±1.0%) for exchange gas pressures greater than 1-cm Hg, and that the agreement is not improved for pressures greater than 10-cm Hg. It should be noted that these results were obtained for time intervals between datum ranging from 1 to 10 minutes. The agreement is considerably improved if longer time intervals are allowed. During the experiments described in Chapters IV and V, time intervals in the order of 20 minutes between temperature changes were used when possible.

For measurements in the 77-350 K range, the outer Dewar is filled with liquid nitrogen, the inner Dewar is filled with helium exchange gas to a pressure of 2-cm Hg above atmospheric pressure, and the sample chamber is filled with exchange gas to a pressure of 10-cm Hg. When the temperature stabilizes at liquid nitrogen temperature, data are taken and the temperature is incremented by applying current to the sample oven by means of a 50 volt, 0.5 amp power supply built for this purpose. When the temperature stabilizes at the new point, data are taken and the temperature is changed again in the same manner.

For measurements in the 4.2-77 K range, liquid helium is transferred into the inner Dewar after the temperature stabilizes at the

liquid nitrogen point with 10-cm Hg of exchange gas in the sample chamber. When the temperature stabilizes at the liquid helium point, data are taken. The exchange gas pressure which is 10-cm Hg at liquid nitrogen usually reduces to approximately 6-cm Hg at liquid helium. After the liquid helium data are taken the exchange gas is pumped out to approximately 6-mm Hg and the oven is utilized to obtain temperature points between 4.2 and 25 K. The exchange gas pressure is reduced to 6-mm Hg because higher pressures cause violent convection currents in the sample chamber which produce large random deviations in the balance displacements. It is not possible to reach temperatures above 25 K using the oven as described above because the liquid helium boils away too rapidly. It requires an entire Dewar of liquid helium to obtain data at 25 K.

When the liquid helium boils away at 25 K it is possible to trap the temperature there by turning off the oven current and turning on the vacuum pump to the inner Dewar. By applying small impulses of current to the oven, stable points between 25 K and 77 K can be obtained.

For measurements below 4.2 K, the temperature is reduced by lowering the vapor pressure of the liquid helium with a vacuum pump. The lowest temperature obtainable in this manner is approximately 0.77 K. Temperatures below 1.5 K are achieved by pumping on the liquid helium when the liquid level is in the tail section of the Dewar where the surface area is greatly reduced. The temperature is changed by changing the helium vapor pressure by means of a large shut-off valve and a by-pass needle valve between the helium Dewar

and vacuum pump. The sample oven is utilized to reach equilibrium conditions more rapidly. The exchange gas pressure, which is near 6-cm Hg at 4.2 K, reduces to approximately 2-mm Hg at the lowest temperatures.

The temperature points in this low temperature region are exceptionally stable. It is possible to select any desired increment of temperature and the temperature chosen can be maintained as long as necessary since a Dewar of helium lasts for several hours when working in this temperature region.

At low temperatures any water vapor in the sample chamber freezes and some of it collects on the sample. A liquid nitrogen cold trap is placed directly behind the helium gas inlet value (the main source of water vapor). The cold trap is very effective in keeping the system free of water vapor.

Experimental Procedure

The equation for the torque acting on a magnetically anisotropic sample in a homogeneous magnetic field is[22]

$$L_M = \frac{m}{2}(\Delta\chi)H^2\sin 2\theta, \tag{23}$$

where m is the mass of the sample, $\Delta\chi \equiv \chi_\perp - \chi_{//}$, H is the field strength, and θ is the angle between the field direction and the c-axis of the crystal. Instead of finding this torque from the angle of rotation and the torque constant of the fiber in order to obtain $\Delta\chi$, there are at least three other ways in which the electrometer can be used to measure $\Delta\chi$.

The first method for measuring $\Delta\chi$ is as follows. The sample is attached to the quartz suspension rod with the c-axis perpendicular to the rotational axis of the balance and lowered into the hang-down tube and Dewar assembly. These components are then positioned under the raised balance, the suspension rod is hooked to the rod attached to the vane of the balance, and the balance is lowered into place. The entire system is aligned so that the sample hangs freely between the pole-pieces of the magnet and the balance has proper alignment with the optical system.

The vacuum connections are made and the sample chamber is evacuated, then filled with helium exchange gas to the desired pressure. Electrical connections to the balance are made, however the quadrant voltage is grounded so that no torque is applied to the system. The light source for the optical system is turned on and the optics are aligned and focused with the mirror on the balance so that a sharply-defined and well-lighted image of the hairline is projected onto the scale. By means of the manual control at the top of the bell jar the electrometer is adjusted for zero reading on the scale. At this time the vane of the electrometer should be hanging symmetrically between the quadrants. In order to check this configuration, the vane voltage selector is set to $V_q/2$ and the quadrant voltage is varied from 0 through 360 volts. From Eq. (20) the electrical torque should be zero for these voltages. If any deflection is noted the entire balance is rotated, then re-zeroed, and the above procedure is repeated. When the zero torque condition prevails the vane-quadrant configuration is correct and all of the adjustment screws are tightened.

The balance voltages are cut off and the magnet is turned on. The magnet current is increased until a pronounced deflection is obtained on the scale. The amount of current necessary for this depends on the sample being used. The voltages are turned on and adjusted for a counter-torque large enough to start the balance deflection back toward the zero point. The magnet is rotated until a maximum deflection is obtained, then the magnet is locked into that position. The electrical counter-torque is used to prevent the sample from merely following the magnet as it is rotated; the torsion fiber used is so sensitive that its counter-torque alone is not enough to prevent this from happening.

The magnet is turned off and voltages are applied to the balance which are to be kept constant during a data run. The voltages are chosen to produce a torque in the opposite direction to the magnetic torque. The magnitude of the electrical torque must not exceed the smallest magnetic torque available over the temperature range of the data run. The magnet is turned on and the current is varied until the counter-torque exerted by the field is equal to the torque applied by the electrometer and there is zero deflection on the scale. At this time the torsion fiber is at equilibrium and the electric and magnetic torques are equal in magnitude but opposite in direction. The value of the magnetic field strength as read by a model 3265 Universal gaussmeter is recorded along with the time, the temperature, and the voltages applied to the balance. The temperature of the sample is then changed and the torque nulling procedure is repeated at the new temperature.

The voltages are kept constant and the sample is always rotated to the same position in the field so that θ is the same for each measurement. Therefore, from Eqs. (20) and (23), $(\Delta\chi)H^2$ is a constant and for two temperatures

$$(\Delta\chi)_{T_1} H^2_{T_1} = (\Delta\chi)_{T_2} H^2_{T_2} \quad . \tag{24}$$

If $\Delta\chi$ is known for some reference temperature, T_R, then $\Delta\chi$ at any other temperature is

$$\Delta\chi_T = \left(\frac{H_R}{H_T}\right)^2 \Delta\chi_R, \tag{25}$$

where $\Delta\chi_R$ is the anisotropy at the reference temperature. Using a value of $\Delta\chi_R$ obtained from Faraday measurements at T_R, $\Delta\chi_T$ can be determined. This method of finding $\Delta\chi$ will be referred to as the "constant voltage method."

In the second, or "constant field," method the magnetic field is kept constant and the voltages applied to the balance are varied for zero deflection. Hence for a single measurement

$$\frac{m}{2}(\Delta\chi)_T H^2 \sin 2\theta = -cV_q(V_v - V_q/2)_T. \tag{26}$$

Since the field and the angle θ are kept constant, a reference temperature measurement gives

$$\Delta\chi_T = \frac{V_q(V_v - V_q/2)_T}{V_q(V_v - V_q/2)_R}\,\Delta\chi_R, \tag{27}$$

and again, if $\Delta\chi_R$ is known, $\Delta\chi_T$ can be determined.

It is sometimes necessary to vary both the voltage and the magnetic field during a run. This is done if $\Delta\chi$ changes sign during a run, if $\Delta\chi$ changes considerably in magnitude during a run, or if $\Delta\chi$ becomes so large that for a given field value, the electrical counter-torque requires such high voltages that arcing occurs between the vane and quadrants via the helium exchange gas. Changing the exchange gas pressure disturbs the thermal equilibrium of the system, hence this is not used as a remedy for the arcing problem. If both the field and voltages are varied during a run the expression for $\Delta\chi$ is

$$\Delta\chi_T = \frac{V_q(V_v - V_q/2)_T}{V_q(V_v - V_q/2)_R}\,\left(\frac{H_R}{H_T}\right)^2\,\Delta\chi_R. \tag{28}$$

In the experiments described later it was the usual practice to take four data readings at each temperature and average these for the final data at that point.

For these experiments $\Delta\chi_R$ was obtained from Faraday measurements on the samples at the temperature of liquid helium under atmospheric pressure. This temperature was used for the reference measurements because it is easily and accurately reproduced, and because the susceptibilities are larger at this temperature than at the liquid nitrogen or room temperature stable points.

The Faraday measurements were made by D. J. Arnold with a Cahn

RG2000 Electrobalance. The balance and the experimental procedure are described in his thesis.[23]

Sample Preparation

The V^{3+} doped sample was grown by the flame-fusion method by D. S. McClure at the RCA Laboratories, Princeton, New Jersey. The sample was used by McClure in his studies of the optical spectra of transition-metal ions in corundum,[6] and then used by C. C. Lin, et al. at the University of Oklahoma for susceptibility studies.[24]

The Ti^{3+} doped sample was grown by the Linde Division of Union Carbide for C. R. Quade who made susceptibility measurements on it for three temperatures at the University of Delaware.[25]

The samples were oriented by x-ray back reflection techniques. The V^{3+} doped sample was cut into an approximate cube with 4.5-mm sides and the Ti^{3+} doped sample was cut with rectangular sides of approximately 7 x 5.5 x 5-mm. Both samples were cut so that the c-axis was perpendicular to a face of the crystal. The samples were heat treated at 1200 C for 24 hours, then highly polished with Silicon Carbide, No. 240-grit grinding paper on a crystal polishing machine. The samples were then boiled in distilled water, boiled in methanol, and weighed. The V^{3+} and Ti^{3+} samples weighed 266.40 mg and 469.06 mg, respectively.

The samples were heat treated because preliminary measurements showed their susceptibilities to have an apparent field dependence. It was thought that there may be clusters of magnetic ions in the crystals whose interactions gave rise to a permanent magnetic moment.

If this were the case, heat treating the crystals might cause these clusters to break up and cause some diffusion of the ions through the crystal. The results of the heat treatment are discussed in the next two chapters.

It was found that some materials used to attach the samples to the quartz rod were magnetic. In some cases even the quartz rods were found to contribute to the susceptibility. These contributions exhibited both anisotropy and field dependence, and although they were small, they were significant in regions where the anisotropic paramagnetic susceptibility of the samples was small.

In particular, No. 36 copper wire made by Belden Mfg. Co. and Eastman 910 adhesive, both of which had previously been used to attach the samples, were found to exhibit anisotropic, field dependent susceptibility. The material used to attach the samples in the final experiments was No. 50, mercerized, cotton sewing thread, manufactured by the American Thread Company. This thread showed no measurable magnetic effects at any temperature. The results of the experiments on the materials mentioned above are shown and discussed in the following chapters.

CHAPTER IV

V^{3+} IN CORUNDUM

Theory

Magnetic anisotropy measurements on $Al_2O_3:V^{3+}$ have not been previously made below 4 K where the temperature dependent anisotropy reaches its maximum value and where the temperature independent Van Vleck anisotropy can be rigorously neglected. It was hoped that by extending the anisotropy measurements below 4 K the parameters which govern the anisotropy could be determined more accurately than has been possible by other experiments.

The ground-state configuration of the free V^{3+} ions is $(3d)^2$ with multiplets ^3F, ^1D, ^3P, ^1G, ^1S in order of increasing energy.[26] The triplet, or magnetic, electronic levels are shown in Figure 7. It will be assumed that the crystalline field is primarily cubic with a small trigonal distortion and that the unit cell has a center of inversion so that the symmetry group of the crystal is C_{3V}.[6] It is well known from symmetry considerations that the cubic field partially removes the degeneracy of the multiplets:

$$^3F \rightarrow {}^3T_1 + {}^3T_2 + {}^3A_2, \quad {}^1D \rightarrow {}^1T_2 + {}^1E,$$

$$^3P \rightarrow {}^3T_1, \quad {}^1G \rightarrow {}^1T_1 + {}^1T_2 + {}^1E + {}^1A_1, \tag{29}$$

$$^1S \rightarrow {}^1A_1.$$

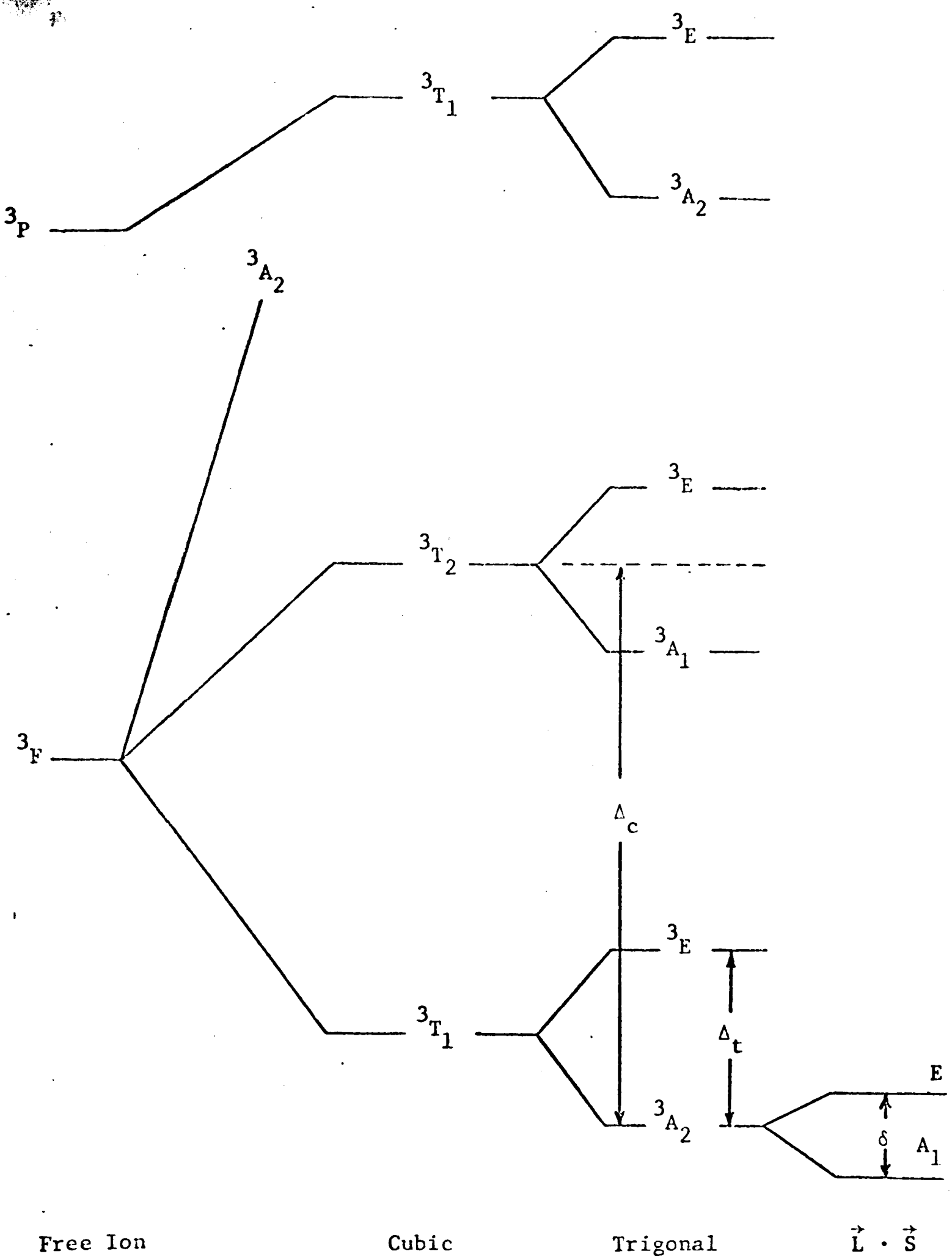

Figure 7. Energy Levels of V^{3+} in a Trigonal Field

Further lifting of the degeneracy by the trigonal component causes the cubic levels to split:

$$^3T_1 \rightarrow {}^3E + {}^3A_2, \qquad {}^3T_2 \rightarrow {}^3E + {}^3A_1, \tag{30}$$

with E, A_1, A_2 unchanged. The $^3T_1$ state in the cubic field is split by the trigonal field into $^3A_2$ and ^3E levels with energy spacing Δ_t. The spin-orbit coupling further splits the $^3A_2$ state into two components separated by δ, the zero-field splitting. This splitting is in second-order and depends on the spin-orbit coupling parameter, λ, and the trigonal splitting of $^3T_1(^3F)$, Δ_t.

The lowest A_1 and E levels with effective spin $S' = 0$ and ± 1, respectively, determine the major part of the paramagnetic susceptibility since only these levels are populated under normal temperature conditions. The g-value which describes the first-order Zeeman splitting of a trigonal level will be anisotropic since components of L + 2S transform according to different representations of C_{3V}.

Quade[24] has obtained the susceptibility expressions for V^{3+} in corundum in the following manner. The matrix elements of the cubic field were calculated using as a basis the functions of the cubic field representation. These functions are linear combinations of the free ion functions for the electronic configuration $(3d)^2$. After diagonalizing the secular equation, the proper wave functions for the ground state in the cubic field were obtained by mixing the $^3T_1$ functions arising from the ^3F and ^3P states. The trigonal field, spin-orbit energy, and magnetic energy were then considered as a small

perturbation. A fourth-order Van Vleck transformation was then applied to remove the matrix elements connecting the $^3A_2$ ground state with the upper states in the trigonal field. After obtaining the energy expressions for the cases of external magnetic field applied perpendicular and parallel to the trigonal axis and substituting into Eq. (19), $\Delta\chi$ was found to be

$$\Delta\chi = A[1 - (1+R/x)\exp(-x)^{-1})] \cdot [1 + 2\exp(-x^{-1})]^{-1} + (\Delta\chi)_{vv}, \qquad (31)$$

where,

$$A = 2N\mu_o^2 g_\perp^2/\delta,\ x = kT/\delta,\ R = (g_{//}/g_\perp)^2. \qquad (32)$$

δ is the zero-field splitting shown in Figure 7. N is the number of vanadium ions, k is Boltzman's constant, μ_o is the Bohr magneton, and T is the absolute temperature. $(\Delta\chi)_{vv}$ is the temperature independent Van Vleck anisotropic susceptibility.[3] The g-factors can be defined by the energy quantum, $g\mu_o H$, associated with magnetic dipole transitions between the Zeeman levels governed by the selection rule $\Delta M = \pm 1$.[1]

Eq. (31) is valid only as long as the temperature is low enough so that the population of the ^3E trigonal state may be neglected. This is estimated to be $T < 600$ K for $\Delta_T \simeq 1000$ cm^{-1}.

The diamagnetic susceptibility of the Al_2O_3 host as well as other isotropic contributions to the susceptibility such as impurities of S-state Mn^{2+} and Fe^{3+} ions, which normally occur as impurities in

Al_2O_3, subtract out of $\Delta\chi \equiv \chi_\perp - \chi_{//}$ and therefore need not be considered.

Experimental Results

The results of the experiments at room temperature on the various materials used to attach the samples to the quartz suspension rod are shown in Figure 8. Using the null method described in the experimental procedure, the equilibrium condition gives

$$\frac{m}{2}(\Delta\chi)H^2\sin 2\theta = -cV_q(V_v - V_q/2), \tag{33}$$

or,

$$\Delta\chi = \frac{-2cV_q(V_v - V_q/2)}{mH^2\sin 2\theta}. \tag{34}$$

If $\sin 2\theta$ is the same for all measurements

$$\Delta\chi = c_1 \frac{V_q(V_v - V_q/2)}{mH^2}, \tag{35}$$

or,

$$\frac{\Delta\chi}{c_1} = \frac{V_q(V_v - V_q/2)}{mH^2}, \tag{36}$$

where c_1 is the constant

$$c_1 = \frac{-2c}{\sin 2\theta}. \tag{37}$$

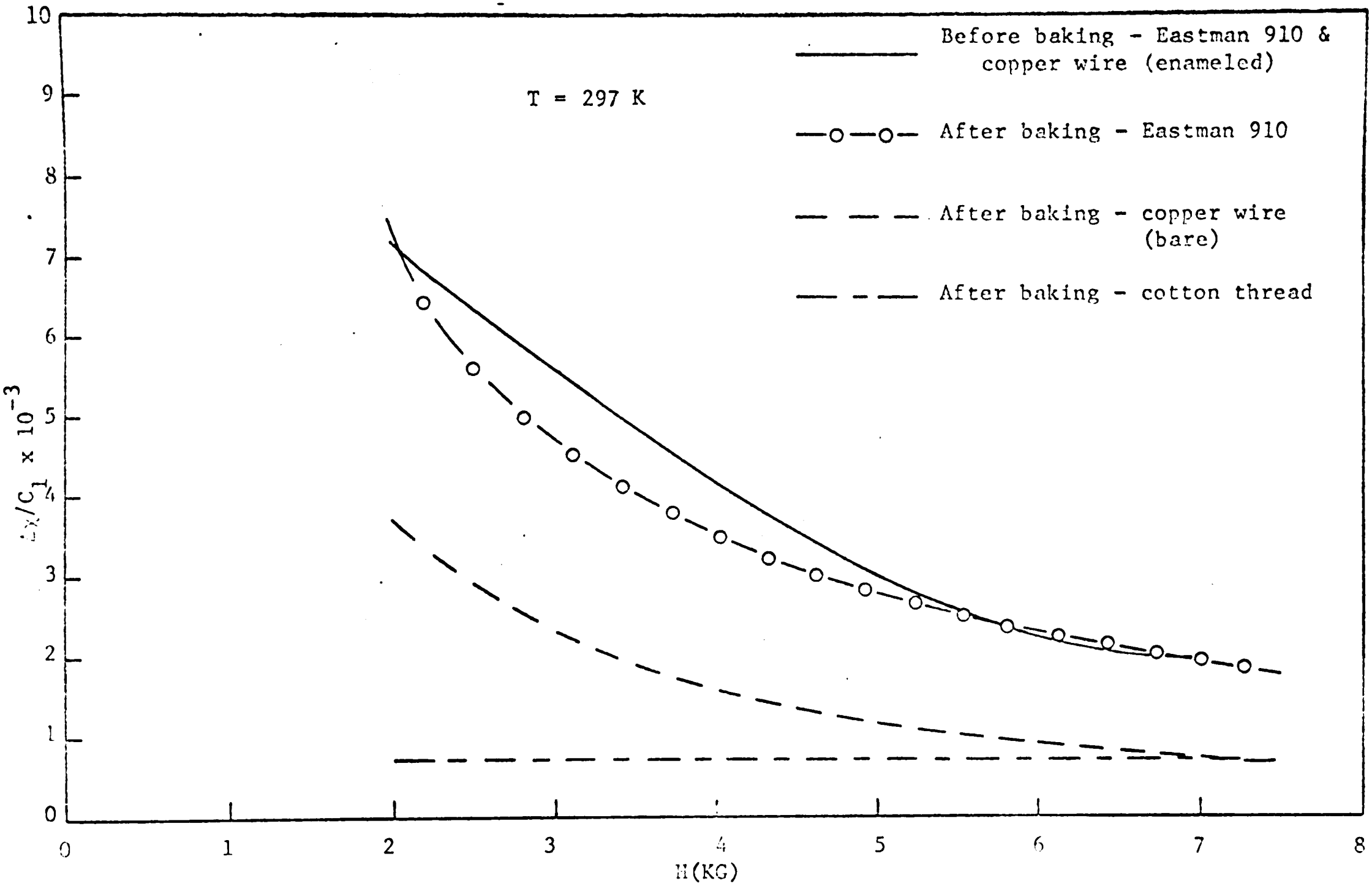

Figure 8. Magnetic Effects of Suspension Materials and Heat Treatment: $Al_2O_3:V^{3+}$.

The mass of the sample was not a constant since the sample was thoroughly lapped and cleaned between each experiment. The results show that both the Eastman 910 glue and the copper wire give significant field dependent contributions to the magnetic anisotropy at room temperature, while the baking process probably had little or no effect. The curve showing the results using cotton thread has been corrected for a small field dependent contribution due to the quartz suspension.

Measurements were also made at liquid nitrogen, liquid helium and pumped liquid helium temperatures, using bare copper wire before baking, and cotton thread after baking. The results support the conclusion that the baking process had negligible effect on the sample. The effects of the suspension materials are masked at low temperatures because of the very large anisotropy of the sample itself, whereas at room temperature the sample anisotropy is quite small. The cotton thread showed no measurable contribution at any temperature and therefore was used in the final experiments.

The results of magnetic anisotropy measurements on the 266.40 mg sample of $Al_2O_3:V^{3+}$ over the temperature range 0.77 to 343.8 K are given in Table 1. The reference value of $\Delta\chi$ obtained from Faraday measurements is $\Delta\chi = (1.158 \pm 0.050) \times 10^{-6}$(cgs-emu/gram-sample) at 4.10 K. The temperature errors have been incorporated into the errors given for $\Delta\chi$. The anisotropy measurements were made by the constant field method and represent the results of at least two independent data runs over all temperature ranges.

Previous measurements of $\Delta\chi$ on this sample have been made by

TABLE 1

Magnetic Anisotropy of $Al_2O_3:V^{3+}$ in units of (10^{-6} cgs-emu/gram-sample)

T(°K)	Δχ	T(°K)	Δχ
0.77	1.712 ± 0.115	11.02	0.178 ± 0.017
0.78	1.711 ± 0.115	12.20	0.144 ± 0.014
0.89	1.791 ± 0.121	14.07	0.099 ± 0.012
1.33	1.744 ± 0.117	15.03	0.080 ± 0.008
1.37	1.698 ± 0.114	15.92	0.072 ± 0.008
1.40	1.749 ± 0.118	17.97	0.052 ± 0.006
1.74	1.722 ± 0.118	20.06	0.037 ± 0.004
1.77	1.677 ± 0.115	20.65	0.037 ± 0.004
2.07	1.688 ± 0.116	21.4	0.033 ± 0.004
2.14	1.635 ± 0.114	22.0	0.030 ± 0.004
2.20	1.670 ± 0.117	22.8	0.026 ± 0.003
2.38	1.589 ± 0.112	23.5	0.024 ± 0.003
2.51	1.585 ± 0.114	24.8	0.021 ± 0.003
2.62	1.534 ± 0.112	25.5	0.018 ± 0.003
2.74	1.530 ± 0.113	28.7	0.014 ± 0.005
2.86	1.476 ± 0.109	36.0	0.006 ± 0.004
2.87	1.500 ± 0.109	41.5	0.000
3.02	1.469 ± 0.110	50.5	−0.002 ± 0.001
3.12	1.415 ± 0.103	59.5	−0.005 ± 0.001
3.26	1.406 ± 0.106	69.6	−0.006 ± 0.001
3.44	1.335 ± 0.105	81.4	−0.005 ± 0.001
3.52	1.332 ± 0.109	101.3	−0.004 ± 0.001
3.66	1.278 ± 0.101	122.2	−0.004 ± 0.001
3.76	1.269 ± 0.105	149.6	−0.003 ± 0.0004
3.90	1.208 ± 0.093	178.2	−0.003 ± 0.0004
4.11	1.177 ± 0.090	200.2	−0.002 ± 0.0003
4.11	1.174 ± 0.090	230.3	−0.002 ± 0.0003
4.11	1.172 ± 0.090	250.4	−0.001 ± 0.0002
4.13	1.153 ± 0.089	273.8	−0.001 ± 0.0002
4.13	1.145 ± 0.089	298.8	−0.001 ± 0.0002
4.13	1.138 ± 0.088	304.9	−0.001 ± 0.0002
4.13	1.177 ± 0.091	343.8	−0.0004 ± 0.0001
4.13	1.146 ± 0.089		
4.13	1.140 ± 0.088		
4.21	1.138 ± 0.091		
4.98	0.905 ± 0.072		
5.00	0.884 ± 0.076		
5.94	0.678 ± 0.058		
7.00	0.504 ± 0.045		
8.01	0.381 ± 0.035		
8.98	0.293 ± 0.027		
9.99	0.227 ± 0.021		

Brumage[24] and by this author.[27] The measurements of Brumage did not extend below 4.2 K, the region where $\Delta\chi$ reaches its maximum value, and where the theoretical expression is most sensitive to the parameters $g_\perp$ and δ. The previous results by this author have been improved by modification of the torsion balance and measurement techniques, which give greater accuracy in the experiment, and by improved analysis techniques, which give more confidence in the reported parameters.

Analysis of Data

The anisotropy data has been analyzed in the temperature region 0.77 - 12.2 K. The analysis was done in this region for three reasons: (1) The anisotropy increases rapidly with decreasing temperature, and reaches a maximum value below 1 K; (2) In this region and especially below 4.2 K, the anisotropy is most sensitive to δ and $g_\perp$, two of the parameters of interest in this study; (3) $(\Delta\chi)_{vv}$ given by,

$$(\Delta\chi)_{vv} \simeq 2N\mu_o^2\alpha^2/\Delta_t \simeq 10^{-9}, \tag{38}$$

in units of (cgs-emu/gram-sample), is negligible compared to the temperature dependent anisotropy below 12 K and therefore can be neglected.

The theoretical expressions for $g_\perp$ and δ as derived by Quade[24] are

$$g_\perp = g - \frac{2\alpha^2\lambda}{\Delta_t} - \frac{\alpha'^2\lambda}{\Delta_c} + \frac{\alpha^2(\alpha-1)\lambda^2}{\Delta_t^2} - \frac{\alpha\alpha'^2\lambda^2}{\Delta_c\Delta_t} + \frac{2\alpha^3(\alpha+1)\lambda^3}{\Delta_t^3}, \tag{39}$$

and,

$$\delta = \frac{\alpha^2\lambda^2}{\Delta_t} - \frac{2\alpha^3\lambda^3}{\Delta_t^2} - \frac{\alpha^4\lambda^4}{\Delta_t^3} - \frac{3\alpha'^2\lambda^2}{2\Delta_c}, \tag{40}$$

where g is the spin-only Lande g-factor with the value g = 2.00229. The parameters α and α' are related to the admixture coefficients between the ^3T, (^3F) functions and the ^3T, (^3P) functions. Their values are $\alpha = 1.29$ and $\alpha' = 1.52$.[24]

If these expressions for $g_\perp$ and δ are substituted into Eq. (31) an expression is obtained for $\Delta\chi$ in which the parameters are λ, $g_{//}$, Δ_c, Δ_t, and N. EPR measurements give $g_{//} = 1.915$;[28] optical data give $\Delta_c = 17{,}400\ cm^{-1}$;[6] and high temperature susceptibility measurements give $\Delta_t = 1100\ cm^{-1}$.[24]

Neglecting $(\Delta\chi)_{vv}$ and forming the ratio $\Delta\chi_T/\Delta\chi_R$, A of Eq. (31) divides out, eliminating the parameter N. Therefore λ is the only remaining unknown parameter explicit in the expression and once it is determined, $g_\perp$ and δ are found from Eqs. (39) and (40).

There were five different methods used to determine the parameters λ, $g_\perp$, δ, and N. The data were analyzed by different methods for three reasons: (1) It is possible to determine different parameters by different methods; (2) comparing results obtained by different methods gives a confidence measure of the results; and (3) the effect of the particular method of analysis upon the results can be studied.

Method 1: $\ell n(\Delta\chi_T/\Delta\chi_R)$ shows remarkable linear behavior for temperatures between 3.00 and 12.2 K. A least-squares fit of $\ell n(\Delta\chi_T/\Delta\chi_R)$

to a straight line gives a slope error of only 0.7%. The slope of $\ell n(\Delta\chi_T/\Delta\chi_R)$ versus T is

$$\frac{d}{dT}\,\ell n\left(\frac{\Delta\chi_T}{\Delta\chi_R}\right) = \frac{d(\Delta\chi_T)}{dx}\,\frac{dx}{dT} = \left(\frac{k}{\delta}\right)\frac{d(\Delta\chi_T)}{dx}/\Delta\chi_T, \tag{41}$$

or,

$$\frac{d}{dT}\,\ell n\left(\frac{\Delta\chi_T}{\Delta\chi_R}\right) = \frac{kc}{\delta}, \tag{42}$$

where,

$$c = \frac{d(\Delta\chi_T)}{dx}/\Delta\chi_T. \tag{43}$$

c is very nearly a constant in the temperature range 3.00 to 12.2 K. The deviation of c is only 4.21% over this range for the values $7.50 \leq \delta \leq 8.50$ and $1.650 \leq g_\perp \leq 1.750$. The variance in c is due almost entirely to $g_\perp$ as it is essentially independent of δ. Calculating c every tenth of a degree for the range of temperatures and parameters indicated, and averaging, gives

$$c = -3.09 \pm 0.13. \tag{44}$$

The slope of the $\ell n(\Delta\chi_T/\Delta\chi_R)$ versus T curve is found from least-squares analysis to be,

$$\frac{d}{dT}\,\ell n\left(\frac{\Delta\chi_T}{\Delta\chi_R}\right) = -0.2673 \pm 0.0018. \tag{45}$$

Substitution of these values into Eq. (42) gives

$$\delta = 8.03 \pm 0.39 \text{ cm}^{-1}. \tag{46}$$

From a calculation of $g_\perp$ and δ over a range of values for λ from Eqs. (39) and (40), the above value of δ gives

$$\lambda = 90.8 \pm 2.7 \text{ cm}^{-1},$$
$$g_\perp = 1.723 \pm 0.007. \tag{47}$$

Method 2: A least-squares fit between the theoretical expression for $\ell n(\Delta\chi_T/\Delta\chi_R)$ and $\ell n[\text{data}(\Delta\chi_T/\Delta\chi_R)]$ was performed in the temperature range 0.77 to 12.2 K using λ as an adjustable parameter, with the results:

$$\lambda = 90.2 \pm 1.5 \text{ cm}^{-1},$$
$$\delta = 7.95 \pm 0.21 \text{ cm}^{-1}, \tag{48}$$
$$g_\perp = 1.723 \pm 0.003.$$

Method 3: A least-squares fit between the theoretical expression for $\Delta\chi_T/\Delta\chi_R$ and the data for $\Delta\chi_T/\Delta\chi_R$ was performed in the temperature range 0.77 to 12.2 K using λ as an adjustable parameter, with the results:

$$\lambda = 92.7 \pm 2.3 \text{ cm}^{-1},$$
$$\delta = 8.31 \pm 0.33 \text{ cm}^{-1}, \tag{49}$$

$$g_\perp = 1.717 \pm 0.006.$$

Method 4: Methods 1-3 give values of the parameters λ, δ, and $g_\perp$ which are independent of the concentration N of vanadium ions in the sample and of the particular value for $\Delta\chi_R$. An average of the results of these three methods gives

$$\lambda = 91.2 \pm 1.0 \text{ cm}^{-1},$$

$$\delta = 8.10 \pm 0.14 \text{ cm}^{-1}, \tag{50}$$

$$g_\perp = 1.721 \pm 0.003.$$

The errors are now average deviations; advantage has been taken of the results of three independent determinations. The anisotropy data, $(\Delta\chi_T/\Delta\chi_R)$, were multiplied by $\Delta\chi_R$ obtained from Faraday measurements. The resulting $\Delta\chi_T$ were least-squares fit to the theoretical expression for $\Delta\chi_T$ over the temperature range 0.77 to 12.2 K using the parameters from Eq. (50) and varying $N\mu_o^2$, giving

$$N\mu_o^2 = (2.37 \pm 0.10) \times 10^{-6} \text{cgs-emu/gram-sample}. \tag{51}$$

Method 5: A least-squares fit between the theoretical expression for $\Delta\chi_T$ and the data for $\Delta\chi_T$ was performed in the temperature range 0.77 to 12.2 K, using $N\mu_o^2$ and λ as adjustable parameters. The results were:

$$N\mu_o^2 = (2.40 \pm 0.10) \times 10^{-6} \text{ cgs-emu/gram-sample},$$

$$\lambda = 92.0 \pm 1.2 \text{ cm}^{-1}. \tag{52}$$

Using this value of λ in the crystal-field expressions for δ and $g_\perp$ gives

$$\delta = 8.21 \pm 0.18 \text{ cm}^{-1},$$
$$g_\perp = 1.720 \pm 0.003. \tag{53}$$

These parameters do depend upon both the vanadium concentration and the reference value for $\Delta\chi_R$.

An average over the results of all five methods then gives

$$N\mu_o^2 = (2.38 \pm 0.10) \times 10^{-6} \text{ cgs-emu/gram-sample},$$
$$\lambda = 91.4 \pm 0.9 \text{ cm}^{-1}, \tag{54}$$
$$\delta = 8.12 \pm 0.14 \text{ cm}^{-1},$$
$$g_\perp = 1.721 \pm 0.002.$$

The errors are again average deviations except for the error in $N\mu_o^2$ which is an average error. The two methods for determining $N\mu_o^2$ are not independent.

All of the least-squares analyses were performed on an IBM-360 computer. Except for Method 1, where the errors were obtained from standard least-squares formulas, the errors were determined from a residue analysis. Expected residues arising from all errors in the experiment were calculated and used as acceptance factors in the parameter determinations.

The data and the theoretical curve are shown in Figure 9. The data error bars are indicative of the experimental errors in the

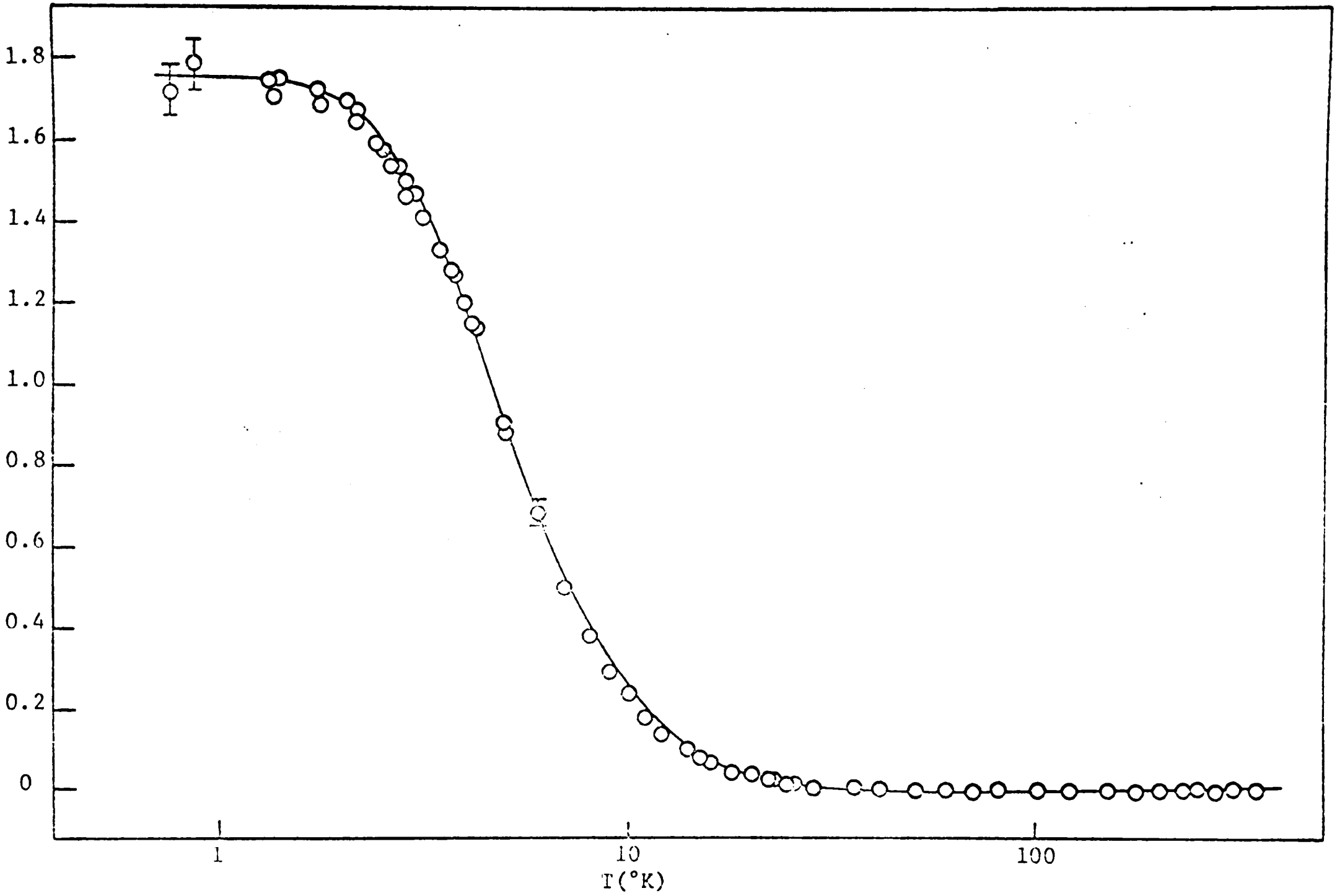

Figure 9. Theoretical and Experimental Magnetic Anisotropy of V^{3+} in Corundum.

respective temperature ranges. Above 10 K the error bars are smaller than the circles used to represent the data. The theoretical curve, indicated by a solid line, was calculated from Eq. (31) using the parameters from Eq. (54) and the values reported from other experiments for the remaining parameters. The units for $\Delta\chi$ are (cgs-emu/gram-sample).

Discussion

The zero-field splitting δ and the perpendicular g-factor $g_\perp$ in $Al_2O_3:V^{3+}$ are quantities which are not readily observed. The zero-field splitting, which is a second order spin-orbit effect, is in the far-infrared spectrum. The perpendicular field splits the doubly degenerate E spin-orbit level only in second order. Values of λ, δ, and $g_\perp$ have been reported by several investigators and a summary of the literature is given in Table 2.

The values of δ obtained from optical and EPR experiments have been generally determined from the temperature variations of the absorption intensity. The difficulty of intensity measurements has greatly limited the accuracy of the values obtained from these sources. Because of the small splitting of the E level with the applied field perpendicular to the c-axis, a direct measurement of $g_\perp$ requires high magnetic fields.

The only parameters reported from magnetic susceptibility measurements are from Ref. (27) and Ref. (24). Reference (27) is work previously reported by this author. The parameters of Eq. (54) are believed to be more accurate than those previously reported for the

TABLE 2

Values for $Al_2O_3:V^{3+}$ Parameters from Other Experiments

Parameter	Value	Experiment*	Reference
$\lambda(cm^{-1})$	95 ± 5	a	24,29
	87 ± 1	a	27
$\delta(cm^{-1})$	8.25 ± 0.02	f	5
	8.4 ± 0.2	a	24
	7.97 ± 0.10	a	27
	8.29	c	30
	8 ± 1	b	31
	7.85 ± 0.4	c	32
	8.3	b	33
	8.3	b	34
	7.9	d	35
	8.26 ± 0.02	e	36
$g_\perp$	1.74 ± 0.02	f	5
	1.720 ± 0.005	a	24
	1.744 ± 0.014	a	27
	1.719	d	35

*a. magnetic susceptibility
b. optical absorption spectra
c. EPR
d. theoretical calculations
e. microwave absorption spectra
f. far-infrared spectra

following reasons: (1) The balance has been modified and the experimental procedures improved, allowing for more accurate measurements; (2) Faraday measurements near 4.2 K have been made to obtain $\Delta\chi_R$. In previous work, $\Delta\chi_R$ was obtained from Ref. (24) as an average of two $\Delta\chi$ measurements taken at 4.2 K, but referenced to Faraday measurements taken at 12 K; (3) The anisotropy measurements have been corrected for errors due to suspension materials.

The errors in the parameters of Eq. (54) seem small for parameters obtained from susceptibility measurements but a simple calculation shows that they are consistent with the errors in the experiment. From Eq. (31) for T < 1 K,

$$\Delta\chi \simeq 2N\mu_o^2 g_\perp^2/\delta. \tag{55}$$

Using the values of Eq. (54),

$$\Delta\chi = \frac{2(2.38 \pm 4.2\%) \times (1.721 \pm 0.1\%)}{8.12 \pm 1.7\%} \text{ cgs-emu/gram-sample}, \tag{56}$$

or,

$$\Delta\chi = 1.736 \pm 6.0\% \text{ cgs-emu/gram-sample}. \tag{57}$$

An average of the three experimental values of $\Delta\chi$ below 1 K from Table 1 gives

$$\Delta\chi_{expt} = 1.738 \pm 6.7\% \text{ cgs-emu/gram-sample}. \tag{58}$$

The error in the calculated value is only slightly less than that of the experimental value. However, the parameters were obtained mostly from $\Delta\chi_T/\Delta\chi_R$ data where the errors were only of the order of 1.5%. The ratio data, and therefore the parameters determined from them, are independent of the 4.3% error in the reference value obtained from Faraday measurements.

The uncertainties in the parameters have been established under the assumption that the Hamiltonian of Eq. (10) is an accurate description of the physical system. The Hamiltonian is, in fact, an approximation and the parameter errors do not reflect the degree of this approximation. The more important interactions which have been neglected in the theory are configuration interactions, covalent bonding, spin-spin interactions, and the dipole-dipole interaction between the nuclear moment and the magnetic moments of the electrons.

McClure[6] has shown that the true site symmetry at the impurity cation is C_3 instead of C_{3v} although the deviation from C_{3v} symmetry is very small. If the array of charges does not have inversion symmetry, odd terms appear in the potential expansion. The matrix elements within the d^n configuration involving the odd terms are still zero, however, such a potential may admix different configurations. The configurations $d^{n-1}p$ lie on the order of 10^5 cm^{-1} above the d^n configurations, so that this mixing is a higher order effect. However, theoretical evidence has been presented to show that the effect may not be negligible.[2]

The simple crystal field theory neglects any orbital mixing between the metal cation and the ligands. However, the experimental

values for no ion of the iron group can be fitted to the theoretical values accurately without considering the effects of covalency.[1] In general, covalent bonding gives rise to the following effects:[1,2]

(a) The term separations of the free-ion are reduced.

(b) The spin-orbit interaction parameter λ is found to be smaller than in the free-ion.

(c) The covalent bond reduces the orbital contributions to the g-factor.

(d) There is a reduction in the second order contribution of the spin-orbit coupling to the g-factor.

(e) The hyperfine structure is reduced.

(f) There may be additional hyperfine interactions between the magnetic electrons and the surrounding nuclei.

Covalent bonding can be explicitly incorporated into the theory by the use of molecular orbitals formed by mixing the d orbitals of the cation with ligand orbitals of appropriate symmetry,[8] or by the introduction of orbital reduction factors.[17] The simple crystal field theory deals with covalency by treating the quantities which are affected by covalent bonding as parameters to be determined from experimental data. For example, the value of λ, the spin-orbit interaction parameter, is found to be 91.4 cm^{-1} for $Al_2O_3:Ti^{3+}$, a reduction of approximately 12% from its free-ion value of 104 cm^{-1}. Thus the d electrons are only on the metal ion about 88% of the time. This is a typical reduction in λ for hydrated transition-metal ions.[2]

The order of magnitude of the spin-spin and electron-nuclei dipole-dipole interactions are 1 cm^{-1} and 10^{-1}-10^{-3} cm^{-1}, respectively.[1]

The spin-spin interaction is comparable in size to the uncertainty in λ which is ± 0.9 cm^{-1}, and the error in $g_\perp$ gives rise to an uncertainty of $\pm 0.3 \times 10^{-3}$ cm^{-1} in the Zeeman splitting, for the field value used in this experiment, which may be comparable to the electron-nuclei interaction.

The simple crystal field model is very successful in establishing the magnitudes of the parameters which arise in the theory as evidenced by the excellent agreement of δ obtained from this work with the values obtained by the most accurate direct measurements. However, the uncertainties in the parameters must be viewed in light of the approximations in the theory. Further improvement in the experiment would not be practical unless the theory is extended to include the interactions which have been neglected because these omissions give rise to theoretical errors which are comparable to the experimental errors in this work.

The errors in the crystal field parameters Δ_c and Δ_t also limit the accuracy of the parameter values reported in this work. The cubic-field splitting Δ_c should affect the parameters only in second order but the effect of Δ_t is large, especially at high temperatures. A direct measurement of Δ_t has not yet been made as the $(t_2^2\ {}^3T_1)\,{}^3A_2 \rightarrow {}^3E$ transition occurs in a region where the corundum lattice absorbs strongly.[37] The value $\Delta_t = 1100$ cm^{-1} obtained from high temperature susceptibility measurements[24] is substantiated by this work. Above 77 K the magnetic anisotropy depends strongly on Δ_t and Figure 9 shows that there is excellent agreement between theory and experiment in the high temperature region when the value $\Delta_t = 1100$ cm^{-1} is used in

the theoretical expression. This agreement is especially satisfying because only the data below 12 K were used in the data analysis to fix the parameters.

$N\mu_o^2$ is smaller than previously reported for the same crystal.[24] This could be due to a more accurate determination because of the difference in the temperature range over which it was determined, or to the fact that only a piece of the original crystal was used, and the V^{3+} concentration may not have been uniformly distributed in the original crystal.

The validity of the simple crystal-field theory is further verified by Macfarlane's[35] calculations. His results (see Table 2) agree very well with the results of this experiment.

CHAPTER V

Ti^{3+} IN CORUNDUM

Theory

The ground state configuration of the free Ti^{3+} ion is $(3d)^1$ which has only a ^2D multiplet. The energy level diagram for the low-lying levels of d^1 impurity systems in corundum is shown in Figure 10.[38] An octahedral field splits the atomic ^2D ground state into a lower orbital triplet ($^2T_{2g}$) and an excited doublet (^2E_g) separated by Δ_c. The trigonal distortion further splits the threefold level into an orbitally twofold degenerate level (^2E) and an orbitally non-degenerate level ($^2A_1$) separated by Δ_t. Finally the spin-orbit interaction leaves three Kramers' doublets in the ground manifold and two in the upper manifold; in Figure 10 these levels are labeled by the symmetries of the trigonal double group.

McClure[6] has reported $\Delta_c = 19050\ cm^{-1}$ and $\Delta_t > 500\ cm^{-1}$ from analysis of the optical absorption data. In determining Δ_c he assumed the trigonal component of the observed splitting to be due to a trigonal splitting of $1000\ cm^{-1}$. The appearance of a double peak in the spectra is evidence for a Jahn-Teller distortion in the excited ^2E_g state which is not split by the trigonal field. The zero-field splittings δ_1 and δ_2 have recently been found to be 37.8 and 107.5 cm^{-1},[5] respectively, from analysis of the far-infrared spectra.

The g-factors for the $E_{3/2}$ ground state have been measured by EPR and far-infrared spectra and found to be $g_{//}^0 = 1.067$ and $g_{\perp}^0 < 0.1$.[5,39] Infrared spectra show the first excited $^1E_{1/2}$ state

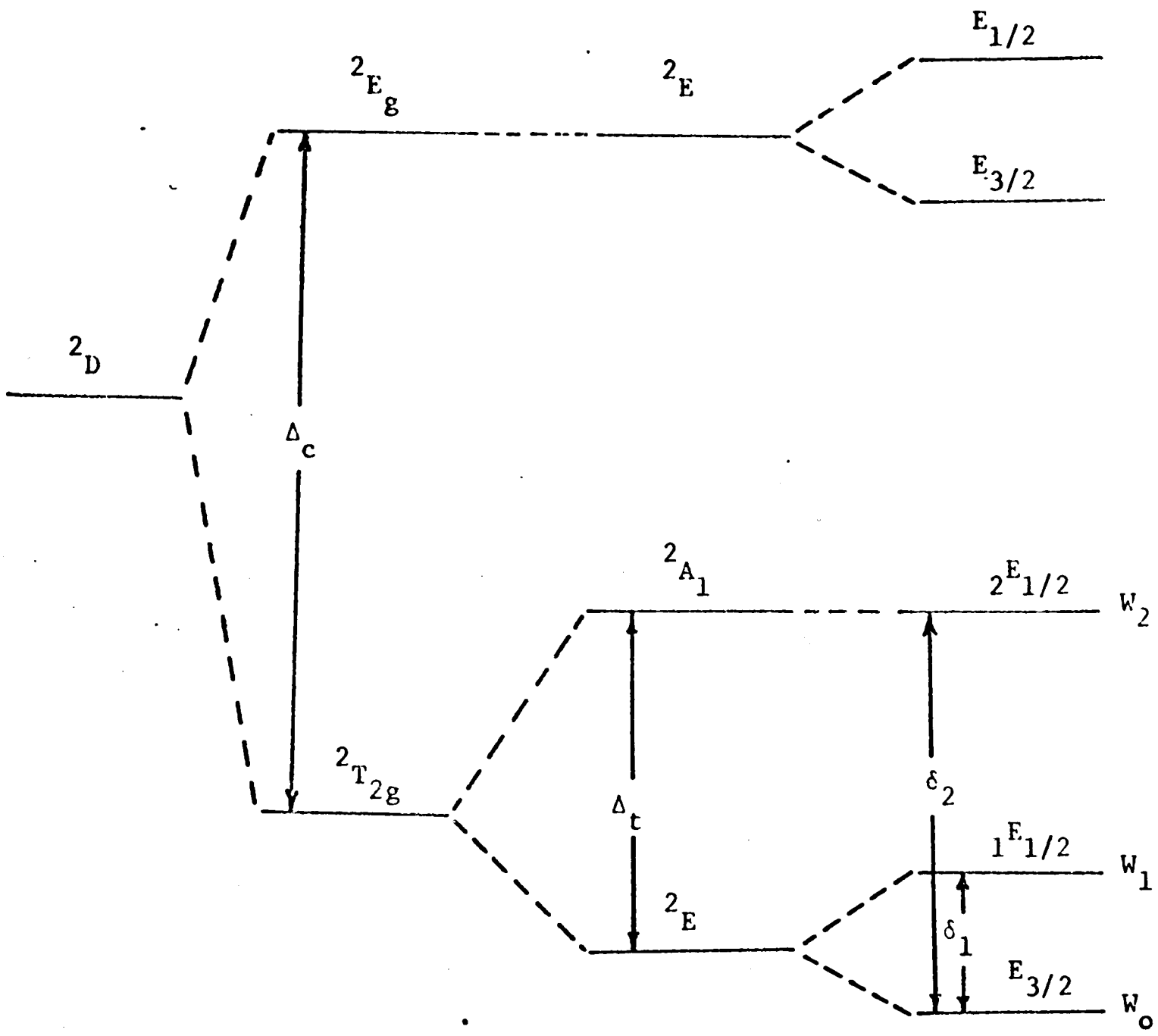

Figure 10. Low Lying Levels of d^1 Impurity Systems in Corundum

g-factors to be $g_{//}^1 = 2.00$ and $g_{\perp}^1 < 0.1$.[5] The second excited $^2E_{1/2}$ state g-factors have not been measured.

The simple crystal field Hamiltonian, Eq. (10), has been applied to d^1 impurity systems by several investigators. The method of solution is in general the same as that discussed for $Al_2O_3:V^{3+}$. Cottrell and Quade[25] have derived theoretical expressions for the magnetic susceptibilities, g-factors, and energy differences in the conventional manner utilizing the crystal-field approximation. Expressions for the zero-field splitting δ_2 and the g-factors for the $^2E_{1/2}$ state were not obtained. These theoretical results were analyzed using scant magnetic susceptibility data but the results were inconclusive as to the importance of covalency or Jahn-Teller interactions which were neglected in the theory.

Gladney and Swalen[40] have diagonalized the Hamiltonian exactly including the interaction with the excited ^2E term, but do not obtain analytical expressions for the final energies of the ground manifold in an applied magnetic field. Therefore the magnetic susceptibility expressions cannot be obtained from their work. They conclude from their work that both the upper manifold contribution and covalency may be important but are not able to estimate the extent of these contributions due to the limited experimental data available to determine the parameters.

Recently, Macfarlane, Wong, and Sturge[38] have investigated the $Al_2O_3:Ti^{3+}$ system using the crystal field model. They have included the interaction with the excited ^2E term and the d^1 energy matrix was diagonalized including both the $^2T_2$ and E terms. Covalency was

included in the model by the introduction of Stevens' orbital reduction factor. The theory was analyzed using the measured value of Δ_c and "typical" values of the spin-orbit parameter λ and the trigonal field parameters. The "typical" values were extrapolated from values of these parameters for other trivalent $3d^n$ ions in corundum. They found that the experimental results could not be explained by the simple static crystalline field model. No reasonable values of the crystal-field parameters allowed reasonable agreement with experimental data. An orbital reduction factor k of 0.5 was needed in order to explain the g-factors. In the usual covalent theory of the orbital-reduction factor,[17] this would imply complete delocalization of the electron onto the neighboring oxygen ions.

It has recently been shown that the dynamic Jahn-Teller effect in a complex having orbital degeneracy may partially quench spin-orbit interaction, the orbital parts of the Zeeman and hyperfine interactions, and other orbital operators governing response to perturbations such as strain or applied electric fields.[18,38,41] The Jahn-Teller interaction may on occasion produce very much greater reductions in orbital parameters in the system than can reasonably be attributed to covalency.

Jahn and Teller[42,43] showed that an electronically degenerate state of a nonlinear complex is unstable (except in the case of simple Kramers' degeneracy) with respect to some asymmetric nuclear displacement which lifts the degeneracy. If the coupling between the electrons and such displacements is sufficiently strong relative to the zero-point energy of the associated vibrational modes, the complex under-

goes a static distortion to a new configuration of minimum energy.[44-46] If the coupling is less strong, or if the zero-point vibrational energy is comparable with the energy barrier separating equivalent configurations, no static distortion occurs, but the complex exhibits a coupled motion of the electrons and the vibrational modes.[47-49] This latter situation is referred to as the dynamic Jahn-Teller effect.[50,51]

The case of a Jahn-Teller interaction that is somewhat stronger than the spin-orbit interaction yet not so strong as to produce a static distortion has been considered for $(3d)^1$ impurity systems in Al_2O_3.[38,41] In particular, Macfarlane, Wong, and Sturge[38] have calculated explicitly the effect of this interaction on the $^2T_2$ ground term, including the small interaction with the excited ^2E term. Inclusion of second-order effects enabled them to obtain quantitative agreement with the measured zero-field splittings and g-values. They obtained analytical expressions for the energy splittings δ_1 and δ_2 as well as the g-values for the Zeeman splittings of the $E_{3/2}$ level. The dynamic Jahn-Teller effect does not alter the splitting scheme but does reduce the level separations.

Unfortunately, the inclusion of vibronic interactions further complicates the theory to an extent that not even approximate analytical expressions have been obtained for the final energies of the three low-lying Kramers' doublets in an applied magnetic field. Therefore, direct analysis of magnetic anisotropy data by the use of the Macfarlane, Wong, and Sturge (MWS) theory is not possible at this time. However, magnetic anisotropy data can be used to confirm the values of the zero-field splittings and g-factors reported from op-

tical and EPR data; to investigate the degree of approximation of the Cottrell-Quade (CQ) theory; and to fix the magnitudes of the temperature independent Van Vleck contributions to the magnetic anisotropy.

To accomplish these aims, an analytical expression for the magnetic anisotropy has been obtained which is independent of any particular theory. It is dependent only upon the validity of the more general Van Vleck theory for paramagnetic susceptibility and the level splitting scheme of Figure 10. Both have been quite well established.

The Van Vleck expression for susceptibility, Eq. (19), has been expanded for the three levels arising from the trigonal $^2T_2$ level in a magnetic field. The resulting expression for $\Delta\chi$ is

$$\Delta\chi = B\{\frac{N\mu_o^2}{4kT}[((g_\perp^o)^2 - (g_{//}^o)^2) + ((g_\perp^1)^2 - (g_{//}^1)^2)\exp(-\delta_1/kT) +$$

$$((g_\perp^2)^2 - (g_{//}^2)^2)\exp(-\delta_2/kT)] + \Delta\chi_{vv}^o + \Delta\chi_{vv}^1 \exp(-\delta_1/kT) +$$

$$\Delta\chi_{vv}^2 \exp(-\delta_2/kT)\}, \qquad (59)$$

where

$$B = [1 + \exp(-\delta_1/kT) + \exp(-\delta_2/kT)]^{-1}. \qquad (60)$$

The following substitutions have been made:

$$W_1^o - W_o^o \equiv \delta_1,$$

$$W_2^o - W_o^o \equiv \delta_2, \tag{61}$$

$$W_i^{(1)} \equiv \pm g^i \mu_o/2, \qquad (i = 0,1,2),$$

$$-2NW_i^{(2)} \equiv \chi_{vv}^i, \qquad (i = 0,1,2).$$

Eq. (59) is used in the analysis of the data.

Experimental Results

Preliminary measurements showed that the magnetic anisotropy of the $Al_2O_3:Ti^{3+}$ sample had a field dependence which could not be attributed to the suspension system. It was thought that heat treating the sample would eliminate the field dependence if it was due to clusters or pairs of interacting magnetic ions in the crystal. The results of heat treating the sample of $Al_2O_3:Ti^{3+}$ are shown in Figure 11. $\Delta\chi/c_1$ has been plotted versus the applied magnetic field for room, liquid helium and pumped liquid helium temperatures. c_1 is given by Eq. (37). The suspension system and material used to attach the sample were the same for all runs. In each case the upper curve represents data taken before baking the sample in air for 24 hours at 1200 C, and the lower curve represents data taken after baking.

It is seen that the heat treatment had some effect on the magnetic anisotropy of the sample, and that except at 1.49 K, the field dependence of the anisotropy was removed by the baking. One expla-

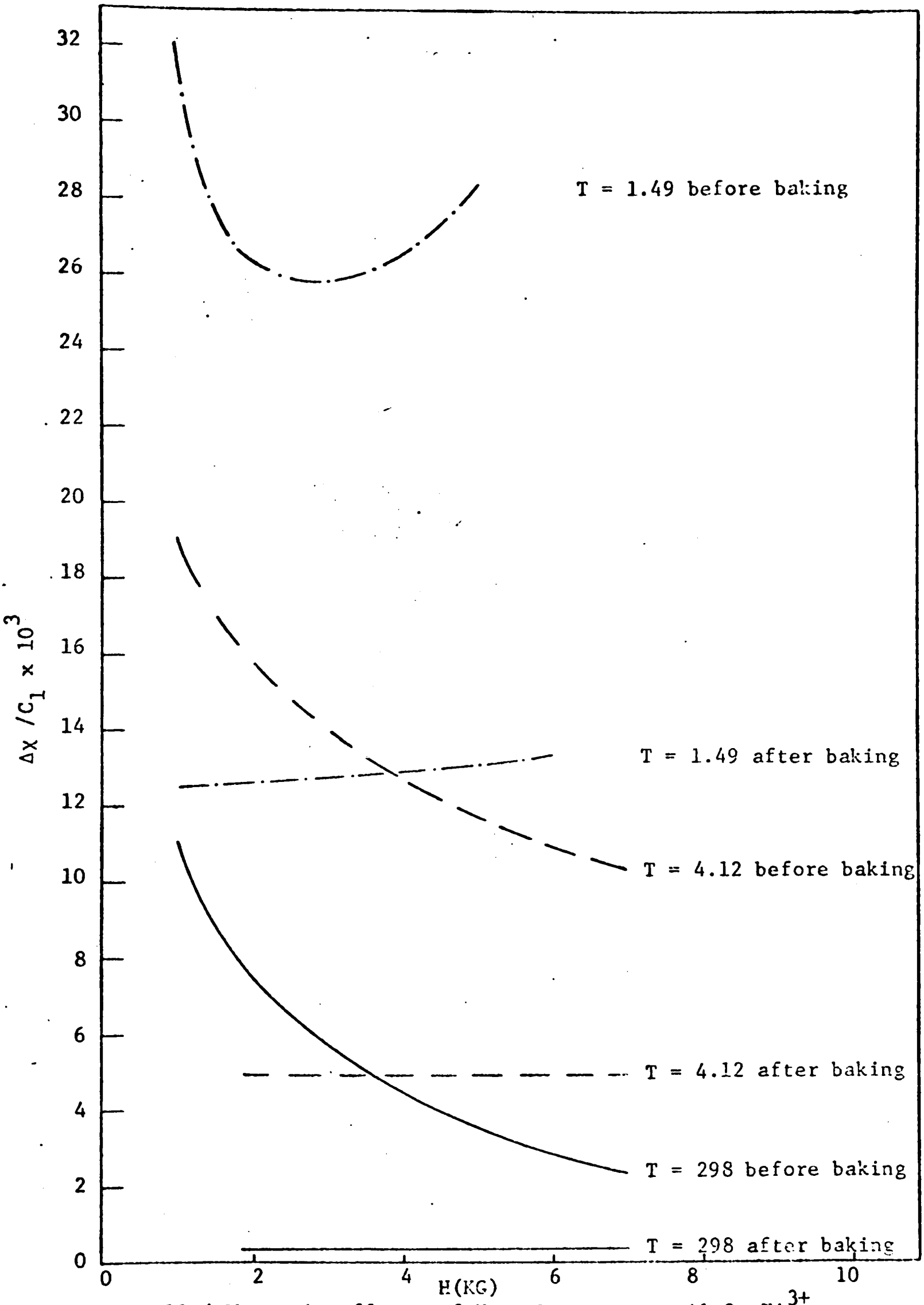

Figure 11: Magnetic effects of Heat Treatment: $Al_2O_3:Ti^{3+}$.

nation for this behavior is that there were pairs or clusters of Ti^{3+} ions in the unbaked sample as a result of the way in which the sample was grown and these were broken up by the heating, and effectively uncoupled except at low temperatures where the weak coupling energy becomes larger than the thermal energy. Bhide and Date[52] have shown that iron clusters can be produced in $Al_2O_3:Fe^{3+}$ by firing the sample in a hydrogen atmosphere at temperatures ranging from 400-1100 C, and that the clusters can be dispersed and become redissolved in the lattice to give Fe^{3+} in Al^{3+} sites when the sample is baked in air for 3 hours at 1050 C.

The assumption of cooperative effects is also strongly supported by the presence of dark bands or striations in the crystal. These bands occur as narrow, parallel layers running perpendicular to the c-axis. It was suspected that these striations resulted from a non-uniform distribution of Ti^{3+} ions with the darker layers being more concentrated than the lighter ones. McClure[6] reported that all of his samples of $Al_2O_3:Ti^{3+}$ contained what appeared to be a cloudy precipitate which he suggested may have been TiO_2. The field dependent behavior at 1.49 K manifests itself in the final anisotropy data and an attempt to analyze this effect is made in the next section.

The results of magnetic anisotropy measurements on the 569.06 mg sample of $Al_2O_3:Ti^{3+}$ are given in Table 3. The reference value of $\Delta\chi$ obtained from Faraday measurements is $\Delta\chi = (-0.0411 \pm 0.005 \times 10^{-6}$ (cgs-emu/gram-sample) at 4.13 K. The temperature errors have been incorporated into the errors for $\Delta\chi$. The anisotropy measurements were made by the constant field method and represent the results of at

TABLE 3

Magnetic Anisotropy of $Al_2O_3:Ti^{3+}$ in Units of (10^{-8} cgs-emu/gram-sample).

T(°K)	Δχ	T(°K)	Δχ
1.10	7.41 ± 1.08	8.99	1.34 ± 0.24
1.12	7.44 ± 1.09	9.55	1.23 ± 0.25
1.37	7.59 ± 1.09	10.00	1.13 ± 0.22
1.38	7.56 ± 1.09	11.00	1.01 ± 0.19
1.44	7.65 ± 1.10	11.98	0.91 ± 0.18
1.53	7.58 ± 1.11	14.06	0.77 ± 0.14
1.73	7.49 ± 1.08	16.00	0.72 ± 0.14
1.80	7.32 ± 1.05	18.04	0.70 ± 0.12
2.00	7.34 ± 1.06	20.08	0.70 ± 0.15
2.26	6.97 ± 1.00	21.49	0.79 ± 0.17
2.30	6.89 ± 1.06	24.68	0.78 ± 0.24
2.48	6.54 ± 1.04	30.8	0.86 ± 0.24
2.76	6.02 ± 1.01	40.0	0.99 ± 0.17
2.82	5.84 ± 0.97	50.6	1.08 ± 0.18
3.00	5.62 ± 0.91	60.2	1.56 ± 0.24
3.25	5.17 ± 0.85	70.1	1.21 ± 0.24
3.30	5.11 ± 0.85	80.8	1.23 ± 0.19
3.50	4.86 ± 0.82	82.8	1.16 ± 0.20
3.78	4.48 ± 0.80	83.0	1.25 ± 0.22
3.80	4.43 ± 0.74	83.1	1.23 ± 0.20
4.06	4.14 ± 0.67	99.8	1.26 ± 0.21
4.08	4.10 ± 0.65	106.0	1.20 ± 0.21
4.10	4.14 ± 0.65	149.8	1.22 ± 0.20
4.12	4.09 ± 0.65	200.0	1.28 ± 0.21
4.12	4.14 ± 0.66	250.0	1.27 ± 0.20
4.12	4.13 ± 0.64	302.2	1.20 ± 0.19
4.12	4.14 ± 0.67	342.4	1.19 ± 0.20
4.16	4.01 ± 0.64		
4.31	3.84 ± 0.75		
4.51	3.56 ± 0.58		
4.99	3.14 ± 0.50		
5.00	3.26 ± 0.55		
5.48	2.77 ± 0.44		
6.00	2.45 ± 0.45		
6.46	2.21 ± 0.38		
7.00	1.98 ± 0.34		
7.48	1.79 ± 0.33		
7.50	1.76 ± 0.33		
7.99	1.60 ± 0.29		
8.50	1.46 ± 0.26		

least two independent data runs over all temperature ranges.

The magnetic anisotropy of $Al_2O_3:Ti^{3+}$ has not previously been reported in the literature. A very sensitive balance is required for these measurements as the anisotropy is almost two orders of magnitude smaller than that for $Al_2O_3:V^{3+}$. The torsion data of the form $(\Delta\chi_T/\Delta\chi_R)$ is considered to have an accuracy on the order of ±2% over most of the temperature range. The large errors in the data of Table 3 are mostly a consequence of an error of 13% in the reference value for $\Delta\chi$ at 4.13 K. This is due to the small anisotropy, causing a large error in the difference $\Delta\chi = \chi_\perp - \chi_{//}$. A reference value for $\Delta\chi$ for a temperature lower than 4.13 K, where the anisotropy is larger, could not be obtained from Faraday measurements because of large errors in the measurements introduced by instabilities in the system.

Analysis of Data

In the equation for $\Delta\chi$, Eq. (59), the unknown parameters are N, $\Delta\chi^0_{vv}$, $\Delta\chi^1_{vv}$, $\Delta\chi^2_{vv}$, and $[(g^2_\perp)^2 - (g^2_{//})^2]$. It was possible to determine all of these parameters by analyzing the data in three temperature regions. For $T \leq 10$ K the contributions from the first and second excited states are negligible, therefore only the expression for the ground state anisotropy was used to analyze the data in this region. For $T \leq 40$ K the contribution from the second excited state is negligible and this state is neglected in the analysis. For $T > 40$ K all three states are considered. The analysis will be presented for each temperature region.

Region 1; $T \leq 10$ K: The expression for $\Delta\chi$ in this region is

$$\Delta\chi_o = \frac{-N\mu_o^2 (g_{//}^o)^2}{4kT} + \Delta\chi_{vv}^o, \tag{62}$$

for $g_\perp^0 = 0$. Theory gives $g_\perp^0 = 0$[25,38] and EPR and optical data give $g_\perp^0 < 0.1$.[39,5] Using the measured value $g_{//}^0 = 1.067$, a least-squares fit was made between the data and a Curie law of the form $\Delta\chi = (a/T) + b$ with the results,

$$N = (1.07 \pm 0.15) \times 10^{18} \text{ per gram-sample}, \tag{63}$$

$$\Delta\chi_{vv}^o = (6.5 \pm 1.4) \times 10^{-9} \text{ cgs-emu/gram-sample}.$$

Region 2; $T \leq 40$ K: In this region the expression for $\Delta\chi$ is

$$\Delta\chi_{0,1} = [\frac{N\mu_o^2}{4kT}(-(g_{//}^o)^2 - (g_{//}^1)^2 \exp(-\delta_1/kT)) + \Delta\chi_{vv}^o +$$

$$\Delta\chi_{vv}^1 \exp(-\delta_1/kT)] \times [1 + \exp(-\delta_1/kT)]^{-1}, \tag{64}$$

for $g_\perp^1 = 0$. Theory and experiment give $g_\perp^1 = <0.2$ and <0.1, respectively[38,5] Using the measured values for $g_{//}^0$, $g_{//}^1$, and δ_1, and the values obtained above for N and $\Delta\chi_{vv}^0$, a least-squares fit was obtained between Eq. (64) and the data for $T \leq 40$ K with $\Delta\chi_{vv}^1$ as the adjustable parameter. The result is

$$\Delta\chi_{vv}^1 = (-3.8 \pm 0.8) \times 10^{-8} \text{ cgs-emu/gram-sample}. \tag{65}$$

Region 3; $T > 40$ K: The expression for $\Delta\chi$ in this region is

given by Eq. (59). A two-parameter least-squares fit between all of the data and this expression, using measured values for the parameters, $g_{\perp}^{0} = g_{\perp}^{1} = 0$, and the results from regions 1 and 2, gives

$$\Delta\chi_{vv}^{2} = (-2.3 \pm 0.5) \times 10^{-9} \text{ cgs-emu/gram-sample}, \qquad (66)$$

$$(g_{\perp}^{2})^{2} - (g_{//}^{2})^{2} = -0.40 \pm 0.05.$$

The errors for the parameters obtained from region 1 were determined from standard least-squares formulas. The errors for the parameters obtained from regions 2 and 3 were obtained by assuming the random error to be as large as the random error for region 1 and also incorporating into the data the errors in the experiment and performing least-squares analyses on the corrected data to find how the parameters changed due to error corrections. All of the parameters determined from this analysis are then:

$$N = (1.07 \pm 0.15) \times 10^{18} \text{ per gram-sample},$$

$$\Delta\chi_{vv}^{o} = (6.5 \pm 1.4) \times 10^{-9} \text{ cgs-emu/gram-sample}, \qquad (67)$$

$$\Delta\chi_{vv}^{1} = (-3.8 \pm 0.8) \times 10^{-8} \text{ cgs-emu/gram-sample},$$

$$\Delta\chi_{vv}^{2} = (-2.3 \pm 0.5) \times 10^{-9} \text{ cgs-emu/gram-sample},$$

$$(g_{\perp}^{2})^{2} - (g_{//}^{2})^{2} = -0.40 \pm 0.05.$$

Using these values, and the reported values for the other parameters, the theoretical curve is plotted with the experimental data in Figure 12. Curve (a) is the theoretical expression for the ground state anisotropy; curve (b) is for the ground and first excited state; curve (c) is the expression for all three states. These curves all converge below 10 K. Above 10 K the error bars are smaller than the circles used to represent the data. The units for $\Delta\chi$ are (cgs-emu/gram-sample).

The theoretical curve does not fit the data below about 3 K, but there is excellent agreement above this temperature. Not only does the curve not fit the data below 3 K, but the data behaves in such a way that the theory, which predicts T^{-1} dependence in this region, cannot possibly explain it. The Van Vleck susceptibility formula, Eq. (19), was derived assuming the magnetic energy was much less than the thermal energy. If this condition does not hold the exponentials cannot be expanded and the resulting expression for the susceptibility is dependent upon the applied magnetic field. The expression for the ground state anisotropic susceptibility in this case is

$$\Delta\chi = \frac{-Ng_{//}^{o}\mu_{o}}{2H}\tanh\left(\frac{g_{//}^{o}\mu_{o}H}{2kT}\right) + \Delta\chi_{vv}^{o}. \qquad (68)$$

At 1 K the magnetic energy is $\simeq 0.09$ cm^{-1} for H = 4 Koe, the field value used in the experiment, and the thermal energy is $\simeq 0.7$ cm^{-1}. Therefore Eq. (68) may be more appropriate than Eq. (62) in the low temperature region. Eq. (68) shows that the magnetic anisotropy can

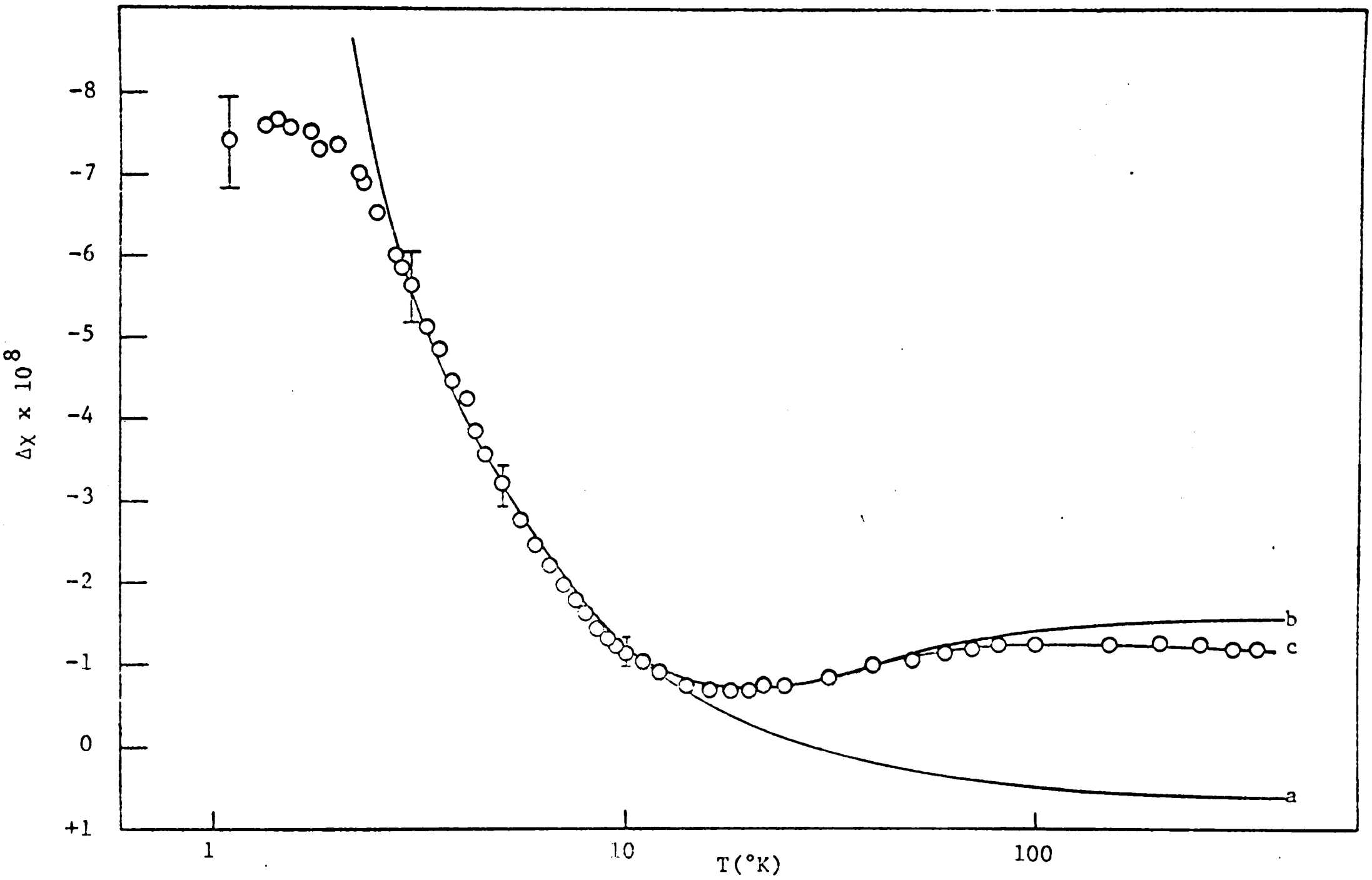

Figure 12. Theoretical and Experimental Magnetic Anisotropy of Ti^{3+} in Corundum.

have a field dependence and a saturation effect at low temperatures. However, Eq. (68) cannot explain the anomolous field-dependent behavior at low temperatures in Figure 11 and cannot fit the data at low temperatures in Figure 12 for the field value used in this experiment. Also there is no appreciable saturation effect evident in the $Al_2O_3:V^{3+}$ data (see Fig. 9) where the magnetic energy is slightly larger and the lowest thermal energy is smaller than for the $Al_2O_3:Ti^{3+}$ data. Therefore, there must be some mechanism besides the single-ion susceptibility giving rise to anisotropy in this region.

The simplest explanation for this anomalous behavior is the presence of exchange effects between magnetic ions, leading to a spontaneous magnetization below an apparent Neél temperature of about 3 K. The model must have the added feature of giving an anisotropic contribution below the Neél temperature and an isotropic contribution above the Neél point.

It was suspected that the anomalous low temperature anisotropy was due to interacting Ti^{3+} ions in the crystal, but Faraday measurements[53] on the $Al_2O_3:Ti^{3+}$ sample suggest another possible source of this anomaly. The Faraday measurements indicated that the sample had a high concentration of unwanted impurities. The data could be explained down to about 3 K assuming that the unwanted impurities were about 25 ppm of sample weight S-state impurities such as Fe^{3+} or Mn^{2+} which are common impurities in Al_2O_3. Therefore, in addition to interacting Ti^{3+} ions with $S = 1/2$, the $S = 5/2$ systems must also be investigated, especially in light of the work of Bhide and Date mentioned above concerning Fe clusters in Al_2O_3. A model developed especially for Fe_2O_3 will be discussed first, then a more general

model will be considered which can be applied to either the S = 1/2 or the S = 5/2 system. These are the only models found in the literature which meet the criteria set forth in the last paragraph.

Moriya[54] has developed a model for anisotropic superexchange interactions and applied it to weak ferromagnetism in Fe_2O_3. The anisotropic superexchange interaction is derived by extending the theory of superexchange interactions to include the effect of spin-orbit coupling. If the crystal symmetry is such that canted spin arrangement is favored rather than a colinear arrangement, anisotropic superexchange results. Using a molecular field approximation the susceptibility expressions were found by Moriya to be,

$$\chi_{//} = \frac{Ng^2\mu_o^2 S(S+1)}{3k(T+T_N)} , \tag{69}$$

$$\chi_{\perp} = \frac{Ng^2\mu_o^2 S(S+1)(T-T_o)}{3k(T+T_N)(T-T_N)} ,$$

with,

$$T_N = \frac{JZS(S+1)}{3k}\left[1+\left(\frac{D}{J}\right)^2\right]^{1/2} , \tag{70}$$

$$T_o = \frac{JZS(S+1)}{3k} .$$

J is the isotropic exchange integral, D is the anisotropic exchange parameter, S is the total spin, and Z is the number of nearest mag-

netic neighbors. Since D/J is small, $(T_N - T_o)$ is small and positive, and the paramagnetic susceptibility increases sharply near T_N. This type of behavior is seen in the $\Delta\chi$ data of Figure 12 at low temperatures. From Eq. (69), $\Delta\chi$ is given by,

$$\Delta\chi = C/(T^2 - \theta^2), \tag{71}$$

where

$$C = \frac{Ng^2\mu_o^2 S(S + 1)(T_N - T_o)}{3k},$$

$$\theta = T_N. \tag{72}$$

Adding Eq. (71) to the expression for the Ti^{3+} single-ion anisotropy for the ground state gives

$$\Delta\chi = \frac{-N\mu_o^2 (g_{//}^o)^2}{4kT} + \Delta\chi_{vv}^o + \frac{C}{T^2 - \theta^2}. \tag{73}$$

Fitting this expression to the data below 10 K by least squares one obtains

$$C = 0.062 \times 10^{-6} \text{ cgs-emu/gram-sample}, \tag{74}$$

$$\theta = 0.750 \text{ K}.$$

These results are shown in Figure 13 as the dashed curve. Below 1 K

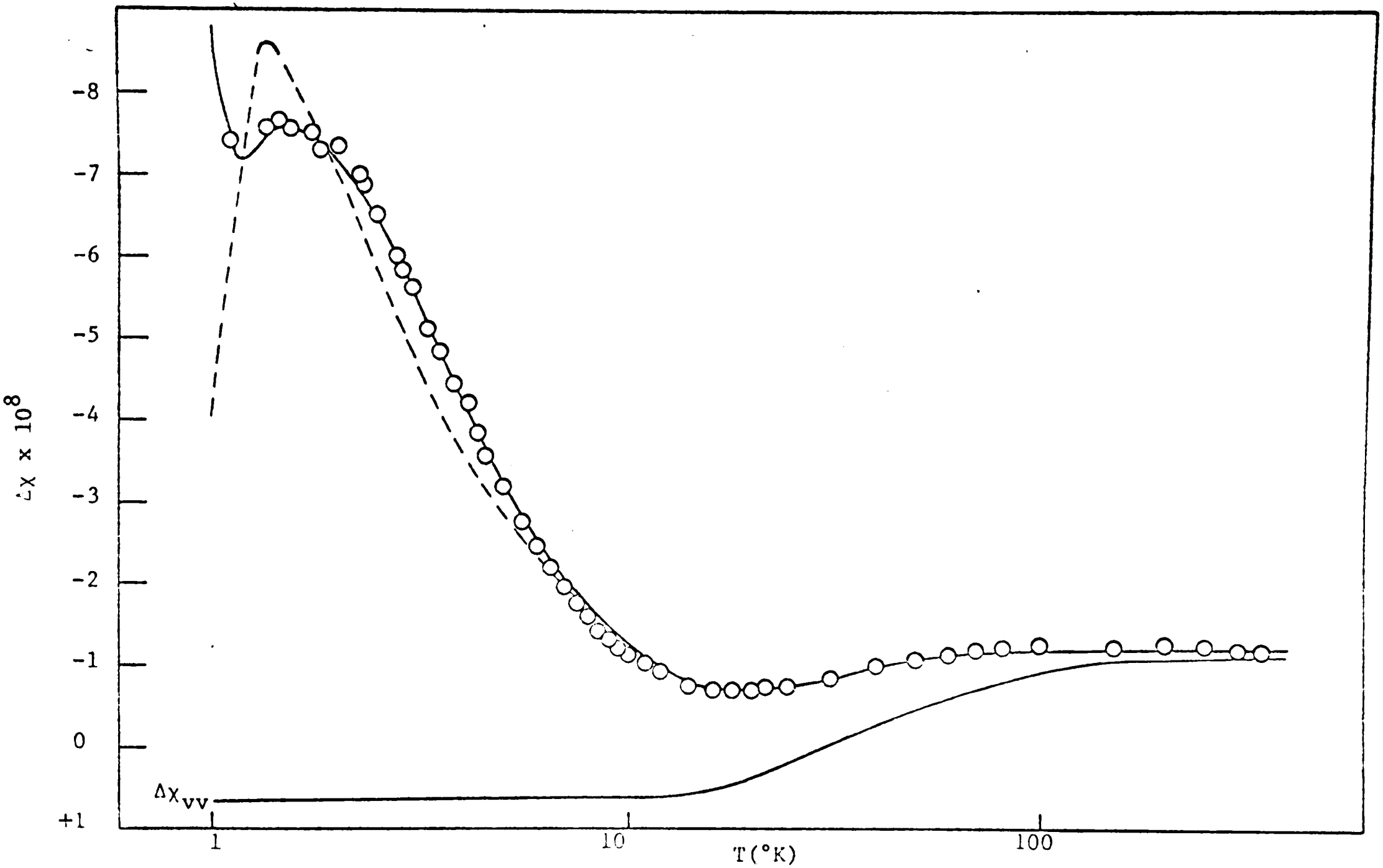

Figure 13. Coupling Theories for Fe^{3+} and Ti^{3+} in Trigonal Fields and Van Vleck Anisotropy for Ti^{3+} in Corundum.

the curve goes to increasing negative values. There is fair agreement between the Moriya model and the data but the correction term does not go to zero fast enough above 3 K. The quantity D/J of Eq. (70) is given by Moriya to be $\simeq 2 \times 10^{-6}$. Using Eq. (70) and the least-squares parameters from Eq. (74) leads to $N_{Fe} \simeq 5 \times 10^{21}$ for the number of Fe^{3+} ions per gram-sample needed to explain the low temperature data with this model. This is unreasonable since the number of Ti^{3+} ions per gram-sample in the crystal is given by Eq. (67) to be $N_{Ti} = 1.07 \times 10^{18}$, and also because the results of Faraday measurements indicate that the upper limit of S-state, S = 5/2 ions per gram-sample is 9×10^{16}.

The second model considered is the Neél-Van Vleck[55] theory for either ferromagnetic or antiferromagnetic materials. This theory predicts an anisotropic susceptibility below the Neél temperature that becomes isotropic above the Neél point. The susceptibility will depend upon the direction of the applied field with respect to the magnetic axes. In the two-sublattice case, the effect of an external field along the magnetic axis is to increase the magnetization of one sublattice and decrease the magnetization of the other. For a perpendicular field, the magnetizations will not be changed (in first order) but both will be rotated slightly away from the axis into the field direction. The expressions for the susceptibilities below the Neél point are,

$$\chi_{\perp} = C/(T_N - \theta),$$

$$\chi_{//} = \frac{C3S(S+1)^{-1}B_S'(\varepsilon/T)}{T - 3S(S+1)^{-1}\theta B_S'(\varepsilon/T)}, \tag{75}$$

where B_S' is the derivative of the Brillouin function, C is the Curie constant, S is the spin angular momentum, and θ is the Curie temperature. Also,

$$\varepsilon = \frac{g\mu_o SnC^{-1}T_N M_j^o}{k}, \tag{76}$$

where n is the number of sub-lattices, T_N is the Neél temperature, and M_j^o is the spontaneous magnetization of the j-th sub-lattice. $\Delta\chi$ is given by

$$\Delta\chi = \frac{C}{T_N - \theta} - \frac{C(1 - \tanh^2 \varepsilon/T)}{T - \theta(1 - \tanh^2 \varepsilon/T)}, \tag{77}$$

assuming that the interacting ions are Ti^{3+} with S = 1/2. For S = 5/2 the corresponding C and θ are $C_{5/2} = 15/7C_{1/2}$ and $\theta_{5/2} = 15/7\theta_{1/2}$. Adding this term to the single-ion anisotropic term and fitting by least squares to the data gives

$$C = 1.80 \times 10^{-10} \text{ cgs-emu/gram-sample},$$

$$T_N = 3.21 \text{ K}, \tag{78}$$

$$\theta = 1.53 \text{ K},$$

$$\varepsilon = 0.79 \text{ K.}$$

The value of $N = 1.07 \times 10^{18}$ per gram-sample for the single Ti^{3+} ions was retained in this analysis. In reality, N and the parameter C of Eq. (77) are interrelated, i.e., N should decrease while C increases as the temperature is lowered. This complicated temperature dependence is neglected in the analysis as it is impossible to determine the numbers of single and coupled ions for a given temperature.

The results of the Neel-Van Vleck model are shown as the solid line in Figure 13. This model fits the data quite well but one cannot infer much physical significance from this since four parameters were used in the analysis. It is not expected that there are any sub-lattices of interacting ions existing throughout the crystal. It is only assumed that regions of interacting sub-lattices exist in the crystal whose net effect is that of some average sub-lattice arrangement. Therefore, n and M_j^o of Eq. (76) are not precisely defined, but this does not affect the quantitative application of the theory since the quantity ε has been taken as an adjustable parameter.

Equating the quantity C of Eq. (77) to $N_{Ti}g^2\mu_o^2S(S + 1)/3k$, given by the Curie-Weiss law of magnetism,[56] and using the least squares value for C given by Eq. (78), the number of interacting Ti^{3+} ions per gram-sample is found to be $N_{Ti} \simeq 3 \times 10^{14}$. Therefore, of the available 1.07×10^{18} Ti^{3+} ions per gram-sample, only 0.03% are needed to explain the low temperature anomaly in the anisotropy. This is a very reasonable result. If the interacting ions are considered to be S = 5/2 ions, it would require approximately 1.4×10^{14} ions per

gram-sample. The results of Faraday measurements indicate that the upper limit of S-state, S = 5/2 ions per gram-sample is 9×10^{16}. It would therefore require a much higher percentage of the available ions to be interacting if the S = 5/2 ions are considered to be the source of the anomaly. In either case, the assumption that the number of single Ti^{3+} ions does not change turns out to be a good approximation.

Also plotted in Figure 13 is the Van Vleck anisotropy for $Al_2O_3:Ti^{3+}$ given by

$$\Delta\chi_{vv} = [\Delta\chi^{o}_{vv} + \Delta\chi^{1}_{vv} \exp(-\delta_1/kT) + \Delta\chi^{2}_{vv} \exp(-\delta_2/kT)] \times$$

$$[1 + \exp(-\delta_1/kT) + \exp(-\delta_2/kT)]^{-1}. \qquad (79)$$

The analytical expression for the magnetic anisotropy obtained from the CQ theory is[25]

$$\Delta\chi = B \frac{N\mu_o^2}{4kT}[(g_{\perp}^{o\,2} - g_{//}^{o\,2}) + (g_{\perp}^{1\,2} - g_{//}^{1\,2}) \exp(-\delta_1/kT)] +$$

$$N\mu_o^2(\frac{2\rho^2}{\delta_1} + \frac{1}{\Delta_t} - \frac{2}{\Delta_c + \alpha_t}) + N\mu_o^2(\frac{1}{\Delta_t} - \frac{2}{\Delta_c + \alpha_t} - \frac{2\rho^2}{\delta_1}) \times$$

$$\exp(-\delta_1/kT)\ , \qquad (80)$$

where,

$$B = [1 + \exp(-\delta_1/kT)]^{-1}, \qquad (81)$$

$$\rho = 1 - \frac{\lambda}{2\Delta_t}\left(1 - \frac{4\alpha_t}{\Delta_c + \alpha_t}\right). \tag{82}$$

The energy splittings Δ_c, Δ_t, and δ_1 are shown in Figure 10. α_t is related to the off-diagonal trigonal field matrix element and λ is the spin-orbit parameter. The superscripts on the g-factors refer to the ground and first excited state. A direct least-squares analysis between Eq. (80) and the anisotropy data is not possible because of the large number of undetermined parameters. There is a minimum of three unknown parameters in the ground state expression for $\Delta\chi$.

Comparing Eq. (80) with Eq. (59) the Van Vleck anisotropies are found to be

$$\Delta\chi^{o}_{vv} = N\mu_o^2\left(\frac{2\rho^2}{\delta_1} + \frac{1}{\Delta_t} - \frac{2}{\Delta_c + \alpha_t}\right), \tag{83}$$

$$\Delta\chi^{1}_{vv} = -N\mu_o^2\left(\frac{2\rho^2}{\delta_1} - \frac{1}{\Delta_t} + \frac{2}{\Delta_c + \alpha_t}\right). \tag{84}$$

Using the values of N, $\Delta\chi^{0}_{vv}$, and $\Delta\chi^{1}_{vv}$ from Eq. (67), given by the $Al_2O_3:Ti^{3+}$ data analysis, and the measured value $\delta_1 = 37.8\ cm^{-1}$, the value of ρ is found from Eqs. (83) and (84) to be

$$\rho = 0.954 \pm 0.0095. \tag{85}$$

The quantity $\Delta_c + \alpha_t$ is given by McClure[6] to be 19400 cm^{-1}, therefore Δ_t could also be obtained from Eqs. (83) and (84). However, the contributions of the terms involving Δ_t and $\Delta_c + \alpha_t$ to the Van Vleck

anisotropy are two orders of magnitude smaller than the contribution of the term involving ρ and it was found that the value of Δ_t obtained from the expressions was very unreasonable. This indicates that the theoretical approximations involved in obtaining the smaller terms has led to appreciable error in their analytic form. To obtain Δ_t, Eq. (82) along with the expression for δ_1 given by

$$\delta_1 = \lambda\left(1 + \frac{4\alpha_t + \lambda}{\Delta_c + \alpha_t} - \frac{\lambda}{2\Delta_t}\right), \tag{86}$$

was used. Eq. (86) was solved for $4\alpha_t/(\Delta_c + \alpha_t)$ and this quantity was substituted into Eq. (82), eliminating the α_t dependence from that equation. The resulting expression is quadratic in $1/\Delta_t$:

$$\left(\frac{\lambda^2}{4}\right)\frac{1}{\Delta_t^2} - \left(\lambda + \frac{\lambda^2}{2(\Delta_c + \alpha_t)} - \frac{\delta_1}{2}\right)\frac{1}{\Delta_t} + (1 - \rho) = 0. \tag{87}$$

Using the measured values $\delta_1 = 37.8\ cm^{-1}$ and $\Delta_c + \alpha_t = 19400\ cm^{-1}$, and $\rho = 0.954$ from Eq. (85), Δ_t was calculated for values of λ ranging from $\lambda = 0.5\lambda_o$ to $\lambda = 0.9\lambda_o$ where $\lambda_o = 153.7\ cm^{-1}$ is the free-ion spin-orbit parameter. The resulting values of Δ_t and the corresponding values of λ were then substituted into Eq. (86) to find corresponding values of α_t. The result of this procedure was a value of Δ_t and α_t for each value of λ, each set of these parameters being consistent with the measured values of δ_1, $\Delta_c + \alpha_t$, and ρ.

The analytical expressions for the g-factors given by the CQ theory are

$$g_{//}^{o} = \frac{4[(2\alpha_t + \lambda)^2 + 2\lambda^2]^{1/2}}{\Delta_c + \alpha_t}, \qquad g_{\perp}^{o} = 0, \tag{88}$$

$$g_{//}^{1} = 4\left(1 + \frac{2\alpha_t - \lambda}{\Delta_c + \alpha_t} - \frac{\lambda^2}{(\Delta_c + \alpha_t)(2\Delta_t - \lambda)}\right), \tag{89}$$

$$g_{\perp}^{1} = \frac{-4\lambda}{2\Delta_t - \lambda}\left(1 - \frac{2\alpha_t + \lambda}{\Delta_c + \alpha_t}\right). \tag{90}$$

The sets of values for λ, Δ_t, and α_t were substituted into these expressions and the g-factors were calculated for each set. The results for $g_{//}^{0}$ were plotted against λ and the value of λ corresponding to the measured value $g_{//}^{0} = 1.07$ was determined to be $\lambda = 0.585\lambda_o = 89.9\ cm^{-1}$. From plots of Δ_t and α_t versus λ the corresponding values of these parameters for $\lambda = 0.585\lambda_o$ were found to be $\Delta_t = 1540\ cm^{-1}$ and $\alpha_t = -2665\ cm^{-1}$. Therefore the set of parameters λ, Δ_t, and α_t consistent with the measured values of ρ, δ_1, and $g_{//}^{0}$ is

$$\lambda = (0.585 \pm 0.082)\lambda_o,$$

$$\Delta_t = 1540 \pm 954\ cm^{-1}, \tag{91}$$

$$\alpha_t = -2665 \pm 30\ cm^{-1}.$$

The errors on these parameters were obtained by changing ρ within its error limits and repeating the calculations described above.

Using the results of Eq. (91) the g-factors for the first excited state were calculated from Eqs. (89) and (90) to be

$$g_{//}^{1} = 2.88 \pm 0.12, \tag{92}$$

$$g_{\perp}^{1} = -0.15 \pm 0.33.$$

From magnetic susceptibility measurements at three temperatures, Cottrell, Andreadakis, and Quade[25] have obtained

$$\rho = 0.85 \pm 0.05,$$

$$\lambda = (0.634 \pm 0.114)\lambda_{o},$$

$$\Delta_{t} = 1250 \pm 750 \text{ cm}^{-1}, \tag{93}$$

$$\alpha_{t} = -3000 \pm 300 \text{ cm}^{-1},$$

$$g_{//}^{1} = 2.55 \pm 0.20,$$

where they have used $g_{//}^{0} = 1.067$, $\delta_{1} = 30 \pm 3 \text{ cm}^{-1}$ and $\Delta_{c} + \alpha_{t} = 19400 \text{ cm}^{-1}$.

Discussion

The Ti^{3+} ion has a single 3d electron in the environment of the corundum lattice. Therefore, of all the crystal field problems one

might expect that the single d-electron problem to be the simplest and the most extensively studied. However, until recently there has not been much progress in the understanding of this system.

Experimental progress has been hampered by the difficulty of growing good single crystals. Ti^{4+} is the most stable charge state and Ti^{3+} is obtained only under controlled conditions. Most investigators of the $Al_2O_3:Ti^{3+}$ system report difficulty due to non-uniform distributions of the Ti ions to an extent that TiO_2 or Ti_2O_3 regions exist in the crystal. Accurate magnetic susceptibility measurements on dilute amounts of Ti^{3+} in Al_2O_3 are difficult due to the small susceptibility of the Ti^{3+} ion and because the Al_2O_3 host and other impurity ions in the crystal have susceptibilities which are not small compared to the Ti^{3+} susceptibility. The extremely small magnetic anisotropy has made accurate anisotropy measurements hard to obtain. Only recently have there been sufficient optical, EPR and far-infrared measurements available to make an analysis of anisotropy data possible.

The theoretical work on $Al_2O_3:Ti^{3+}$ has been difficult because of mechanisms which quench the spin-orbit interaction and the orbital parts of the Zeeman interactions in excess of that which can usually be attributed to covalency. Some investigators have attempted to explain the anomalous quenching by including dynamic Jahn-Teller interactions in the theory. They have had some success in calculating the zero-field splittings and the ground state g-factors, however the difficulty of the calculations has hindered the complete analytical solution to an extent that magnetic susceptibility expressions

have not been obtained. The theoretical work is further hindered by a strong Jahn-Teller distortion in the excited ^2E manifold.

Experimental and theoretical investigators have been able to establish the level splitting scheme for $Al_2O_3:Ti^{3+}$ and this information has been used in conjunction with the Van Vleck theory for paramagnetic susceptibility to analyze very accurate magnetic anisotropy data reported in this work. The analysis has confirmed the values for the zero-field splittings and g-factors for the ground and first excited states reported from EPR and far-infrared measurements. The anisotropy data can be fit extremely well down to about 3 K using the values $\delta_1 = 37.8\ cm^{-1}$, $\delta_2 = 107.5\ cm^{-1}$, $g_{//}^0 = 1.067$, $g_{\perp}^0 = 0$, $g_{//}^1 = 2.00$, and $g_{\perp}^1 = 0$. In addition the difference in the squares of the second excited state g-factors have been found to be $(g_{\perp}^2)^2 - (g_{//}^2)^2 = -0.40 \pm 0.05$ and the Van Vleck anisotropies have been found for all three Kramers' doublets in the ground manifold.

The anomaly in the low temperature anisotropy data has been attributed to the interaction of magnetic ions in the crystal and can be quantitatively explained with the Neél-Van Vleck theory. It was found that the anomaly could not be explained by Brillouin saturation. The analysis was not conclusive as to whether the interacting magnetic ions were $S = 1/2, Ti^{3+}$ ions or $S = 5/2$, S-state ions such as Fe^{3+} and Mn^{2+}.

The Van Vleck anisotropies have been used to analyze the Cottrell-Quade (CQ) theory. This theory was developed in the simple crystal-field approximation and does not include Jahn-Teller interactions or covalency. The effect of covalency or orbital reduction can be

included indirectly by allowing the spin-orbit parameter to deviate from its free-ion value. The CQ theory predicts the ground state zero-field splitting and g-factors in excellent agreement with measured values using $\lambda = 0.59\lambda_o$ cm^{-1}, $\Delta_t = 1540$ cm^{-1}, and $\alpha_t = -2665$ cm^{-1}. The reduction in λ from its free ion value is larger than can reasonably be expected from covalency alone. In the moderately covalent Al_2O_3 host the orbital reduction for transition-metal ions ranges from 10 to 30 percent, for example in the $Al_2O_3:V^{3+}$ analysis it was found to be 12%. The ionic radius of the Ti^{3+} ion is slightly larger than the V^{3+} ionic radius[57] which might account for some additional reduction but it would not be expected to account for all of it.

The values of Δ_t for other transition-metal ions in Al_2O_3 range from 720 to 1950 cm^{-1}.[6] McClure[6] suggests that the variance in these values is due to the difference in ionic radius of the ions which causes different displacements of the ions along the c-axis of the Al_2O_3 host. If this assumption is correct then Ti^{3+} would be expected to have a trigonal field splitting intermediate between $\Delta_t = 1425$ cm^{-1} for Cr^{3+} and $\Delta_t = 1950$ cm^{-1} for Mn^{3+} according to the ionic radii of trivalent transition-metal ions.[57] Therefore the value $\Delta_t = 1540$ cm^{-1} for $Al_2O_3:Ti^{3+}$ obtained from analysis of the CQ theory would be a very reasonable value. The only direct experimental evidence of the magnitude of Δ_t comes from McClure's analysis of the optical absorption spectra which predicts $\Delta_t > 500$ cm^{-1}.

The large value of α_t would indicate a strong trigonal interaction between the $^2T_2$ and ^2E cubic levels. The verification of this must await further experimental and theoretical investigation.

Macfarlane, Wong, and Sturge (MWS) have included the effect of a dynamic Jahn-Teller interaction in the crystal-field theory calculations and were able to predict the zero-field splittings and ground state g-values using $\lambda = 0.8\lambda_o$, $\Delta_t = 700\ cm^{-1}$, and $\alpha_t = -495\ cm^{-1}$. This reduction in λ represents a reasonable expansion of the 3d radial function in Al_2O_3, however, a smaller λ and larger, and perhaps more reasonable, values of the trigonal field parameters would have allowed much better agreement with the crystal field theory excluding the Jahn-Teller interaction with the observed values of δ_1 and $g_{//}^0$. It is not clear that the Jahn-Teller interaction is as important as their results would indicate in explaining the $Al_2O_3:Ti^{3+}$ problem. Neither the CQ theory or the MWS theory are successful in explaining the g-factors for the first two excited levels. The error in $g_{//}^1$ is in excess of 20% for both theories which give $g_{//}^1 = 2.88$ and $g_{//}^1 = -2.5$, respectively, for the CQ and MWS theories. The measured value is $g_{//}^1 = 2.00$. In addition the MWS theory gives the value 0.39 for $(g_{\perp}^2)^2 - (g_{//}^2)^2$ as opposed to -0.40 obtained from this work.

The importance of the dynamic Jahn-Teller interaction in $Al_2O_3:Ti^{3+}$ cannot be established until the covalency effects of this system are better understood. This can perhaps be formally accomplished by a molecular-orbital calculation in which the orbitals are of the form

$$\Psi = \psi(\Gamma) + \sum_i a_i \psi_i, \tag{94}$$

where $\psi(\Gamma)$ is a wave function of the central atom transforming in

the molecular point group as the irreducible representation Γ and $\sum_i a_i \psi_i$ is a linear combination of ligand wave functions transforming according to the same irreducible representation Γ. This formulation is called ligand field theory because it acknowledges the presence of the ligands to a much greater extent than the pure crystal field theory does. In the ligand field theory the structural unit for the wave function is the whole complex ion, rather than the single central atom. In this manner the effects of covalency are built directly into the theory. Once the covalency effects are better understood the role of Jahn-Teller interactions will be more apparent.

For the theoretical investigators who may eventually solve the $Al_2O_3:Ti^{3+}$ problem the Van Vleck anisotropies and the difference in the squares of the $^2E_{1/2}$ g-values reported in this work should be of great help in parameter determinations.

CHAPTER VI

CONCLUSION

The magnetic anisotropies of V^{3+} and Ti^{3+} in corundum have been measured with a sensitive torsion balance in the temperature range 1-350 K.

The anisotropy measurements on $Al_2O_3:V^{3+}$ have been analyzed by the use of theoretical expressions for the anisotropy developed from crystal field theory. The data were analyzed by least-squares methods in the temperature region below 12 K where the Van Vleck anisotropy can be neglected and where the temperature dependent anisotropy reaches its maximum value. The accuracy of the measurements reported here have permitted the determination of the perpendicular g-factor and the spin-orbit coupling parameter with greater accuracy than has been previously possible. Using these parameters in the simple crystal field model the anisotropy over the entire temperature range is predicted in excellent agreement with the anisotropy data. It is shown that increased accuracy in anisotropy measurements would not be practical unless the theoretical work is extended to include interactions which have been neglected.

Anisotropy measurements on $Al_2O_3:Ti^{3+}$ are reported in this work for the first time. The design of the torsion balance used for these measurements has permitted the very small anisotropy of this d^1 impurity system to be determined with exceptional accuracy. Using the Van Vleck theory for paramagnetic susceptibility the data have been

analyzed by least-squares techniques to obtain the Van Vleck anisotropic susceptibilities for all three Kramers' doublets in the ground manifold and the difference in the squares of the g-factors for the $^2E_{1/2}$ level. These quantities along with the g-factors for the other two levels and the zero-field splittings measured by other experiments explain the anisotropy data down to about 3 K. The low temperature anomaly in the anisotropy is accounted for by ferromagnetic coupling between either Ti^{3+} ions or S-state, S = 5/2 accidental impurities in the crystal. Simple crystal field theory can quantatively explain the magnetic properties of $Al_2O_3:Ti^{3+}$ only by assuming a much greater reduction in the spin-orbit coupling parameter than can reasonably be attributed to covalency alone. The large orbital reduction has been explained by some investigators by the inclusion of a dynamic Jahn-Teller effect in the theory but it is argued here that perhaps the Jahn-Teller effect is not as important as previously thought. It is suggested that the use of ligand-field theory would help decide the degree of covalency present in $Al_2O_3:Ti^{3+}$. Until this question is answered it does not seem possible to accurately determine the importance of the dynamic Jahn-Teller effect.

LIST OF REFERENCES

1. W. Low, Paramagnetic Resonance in Solids, (Academic Press, Inc., New York, 1960).

2. D. S. McClure, Electronic Spectra of Molecules and Ions in Crystals, (Academic Press, Inc., New York, 1959).

3. J. H. Van Vleck, The Theory of Electric and Magnetic Susceptibilities, (Oxford University Press, London, 1932).

4. J. S. Griffith, The Theory of Transition-Metal Ions, (Cambridge University Press, Cambridge, 1961).

5. R. R. Joyce, and P. L. Richards, Phys. Rev. 179, 375 (1969). E. D. Nelson, J. Y. Wong, and A. L. Schawlow, Phys. Rev. 156, 298 (1967).

6. D. S. McClure, J. Chem. Phys. 36, 2757 (1962).

7. P. W. Selwood, Magnetochemistry, (Interscience Publishers, Inc., New York, 1956, 2nd ed).

8. C. J. Ballhausen, Introduction to Ligand Field Theory, (McGraw-Hill Book Co., Inc., New York, 1962).

9. R. Schlapp and W. G. Penney, Phys. Rev., 42, 666 (1932).

10. O. Jordahl, Phys. Rev., 45, 87 (1934).

11. H. A. Bethe, Ann. Physik, [5], 3, 133 (1929), English Translation, Consultants Bureau, New York, 1958.

12. J. H. Van Vleck, J. Chem. Phys., 3, 803 (1935).

13. J. H. Van Vleck, J. Chem. Phys., 3, 807 (1935).

14. J. H. Van Vleck and A. Sherman, Revs. Modern Phys., 7, 167 (1935).

15. L. Pauling, The Nature of the Chemical Bond, (Cornell University Press, Ithaca, New York, 1940).

16. E. U. Condon and G. H. Shortly, The Theory of Atomic Spectra, (Cambridge University Press, London and New York, 1953, 2nd ed).

17. K. W. H. Stevens, Proc. Roy. Soc. (London) A219, 542 (1953). See also M. Tinkham, Proc. Roy. Soc. (London) A236, 549 (1956), and W. Low, Ref. 1. pp. 96-103.

18. F. S. Ham, Phys. Rev. 166, 307 (1968).

19. E. C. Kemble, The Fundamental Principle of Quantum Mechanics (Dover Publication, Inc., New York, 1958), p. 394.

20. R. C. Tolman, Statistical Mechanics (Oxford University Press, London, 1938), p. 367.

21. S. G. Starling, Electricity and Magnetism (Longmans, Green and Co., New York, 1925), pp. 157-161.

22. J. F. Nye, The Physical Properties of Crystals (Oxford University Press, New York, 1957), pp. 60-61.

23. D. J. Arnold, High Temperature Magnetic Susceptibilities of Platinum and Palladium Metals (Texas Technological College, 1967, Unpublished M. S. Thesis).

24. W. H. Brumage, C. R. Quade, and C. C. Lin, Phys. Rev. 131, 949 (1963).

25. T. H. E. Cottrell, N. C. Andreadakis, and C. R. Quade, Phys. Rev. Letters 21, 7 (1966).

26. Y. Tanabe and S. Sugano, J. Phys. Soc. Japan 9, 766 (1954).

27. A. R. Smith and R. W. Mires, Phys. Rev. 172, 265 (1968).

28. K. M. Zverv and A. M. Prokhorov, Zh. Eksperim. i Thor. Fiz. 34, 1023 (1958) [English transl.: Soviet Phys.--JETP 7, 707 (1958)].

29. W. H. Brumage, E. C. Segraves, and C. C. Lin, J. Chem. Phys. 42, 3326 (1965).

30. M. Sauzade, J. Pontnau, P. Lesar, and D. Silhouette, Phys. Letters 19, 617 (1966).

31. M. H. L. Pryce and W. A. Runciman, Discussion Faraday Soc. 26, 35 (1959).

32. S. Foner and W. Low, Phys. Rev. 120, 1585 (1960).

33. S. Sokatsume and I. Tsujikawa, J. Phys. Soc. Japan 19, 1080 (1964).

34. W. C. Scott and M. D. Sturge, Phys. Rev. 146, 262 (1966).

35. R. M. Macfarlane, J. Chem. Phys. 40, 373 (1964).

36. E. A. Vinogradov, N. A. Irisova, T. S. Mandel'shtam, A. M. Prokhorov, and T. A. Shmaonov, Pis-ma v Redaksiyu 4, 373 (1966) [English

transl.: Soviet Phys.--JETP Letters 4, 252 (1966)]

37. E. G. Brame, J. L. Margrove, and V. W. Meloche, J. Inorg. Nucl. Chem. 5, 48 (1957).

38. R. M. Macfarlane, J. Y. Wong, and M. D. Sturge, Phys. Rev. 166, 250 (1968).

39. N. E. Kask, L. S. Kornienko, T. S. Mandel'shtam, and A. M. Prokhorov, Fiz. Tverd. Tela 5, 2306 (1963): [translation: Sov. Phys.--Solid State 5, 1677 (1964)].

40. H. M. Gladney and J. D. Swalen, J. Chem. Phys. 42, 1999 (1965).

41. F. S. Ham, Phys. Rev. 138, 1727 (1965).

42. H. A. Jahn and E. Teller, Proc. Roy. Soc. (London) A161, 220 (1937).

43. H. A. Jahn, Proc. Roy. Soc. (London) A164, 117 (1938).

44. J. H. Van Vleck, J. Chem. Phys. 7, 72 (1939).

45. V. Opik and M. H. L. Pryce, Proc. Roy. Soc. (London) A238, 425 (1957).

46. A. D. Liehr, J. Phys. Chem. 67, 389 (1964).

47. W. Moffitt and A. D. Liehr, Phys. Rev. 106, 1195 (1957).

48. W. Moffitt and W. Thorson, Phys. Rev. 108, 1251 (1957).

49. H. C. Longuet-Higgins, U. Opik, M. H. L. Pryce, and R. H. Sack, Proc. Roy. Soc. (London) A244, 1 (1958).

50. F. S. Ham, Spectrochim. Acta. 18, 775 (1962).

51. H. C. Longuet-Higgins, Adv. Spectr. 2, 429 (1962).

52. V. G. Bhide and S. K. Date, Phys. Rev. 172, 345 (1968).

53. D. J. Arnold, Magnetic Susceptibilities of Titanium and Vanadium in Corundum Structures (Texas Tech University, 1970, Unpublished Ph. D. dissertation).

54. T. Moriya, Phys. Rev. 120, 91 (1960).

55. J. H. Van Vleck, J. Chem. Phys. 9, 85 (1941).

56. J. S. Smart, Effective Field Theories of Magnetism, (W. B. Saunders Co., Philadelphia and London, 1966), pp. 80-85.

57. J. B. Goodenough, Magnetism and the Chemical Bond (John Wiley and Sons, New York, 1963), p. 250.